Delft University of Technology

Delft Center for Systems and Control

Technical report 15-042

Distributed MPC for frequency regulation in multi-terminal HVDC grids*

P. Mc Namara, R.R. Negenborn, B. De Schutter, G. Lightbody, and S. McLoone

If you want to cite this report, please use the following reference instead:
P. Mc Namara, R.R. Negenborn, B. De Schutter, G. Lightbody, and S. McLoone, "Distributed MPC for frequency regulation in multi-terminal HVDC grids," *Control Engineering Practice*, vol. 46, pp. 176–187, Jan. 2016. doi:10.1016/j.conengprac.2015.11.001

Delft Center for Systems and Control
Delft University of Technology
Mekelweg 2, 2628 CD Delft
The Netherlands
phone: +31-15-278.24.73 (secretary)
URL: https://www.dcsc.tudelft.nl

* This report can also be downloaded via https://pub.bartdeschutter.org/abs/15_042.html

Distributed MPC for frequency regulation in multi-terminal HVDC grids

Paul Mc Namara[a,*,1], Rudy R. Negenborn[b], Bart De Schutter[c], Gordon Lightbody[d], Seán McLoone[e]

[a] Electronic Engineering Department, Callan Institute, Maynooth University, Kildare, Ireland

[b] Department of Maritime and Transport Technology, Delft University of Technology, Delft, The Netherlands

[c] Delft Center for Systems and Control, Delft University of Technology, Delft, The Netherlands

[d] Control and Intelligent Systems Group, Department of Electrical and Electronic Engineering, UCC, College Rd., Cork, Ireland

[e] Energy, Power and Intelligent Control Research Cluster, School of Electronics, Electrical Engineering and Computer Science, Queen's University Belfast, Belfast, Northern Ireland

Abstract

Multi-Terminal high voltage Direct Current (MTDC) transmission lines enable radial or meshed DC grid configurations to be used in electrical power networks, and in turn allow for significant flexibility in the development of future DC power networks. In this paper distributed MPC is proposed for providing Automatic Generation Control (AGC) in Alternating Current (AC) areas connected to MTDC grids. Additionally, a novel modal analysis technique is derived for the distributed MPC algorithm, which in turn can be used to determine the convergence and stability properties of the closed-loop system.

Keywords: Distributed model predictive control, Convergence, Stability, Modal analysis, Auxiliary problem principle, Automatic generation control, Multi-terminal HVDC

1 Introduction

High Voltage Direct Current (HVDC) links provide significant advantages over Alternating Current (AC) links for transferring electrical energy over large distances (Kundur, 1994). Traditionally HVDC systems have consisted of point to point links that connect two individual AC areas. HVDC links based on Line Commutated Converter (LCC) technology enabled the construction of HVDC grids where a number of individual HVDC lines are connected to an individual HVDC terminal, thus enabling the construction of Multi-Terminal HVDC (MTDC) grids. However, with HVDC LCC power flows in the lines are unidirectional, which limits the flexibility of LCC based MTDC grids. Voltage Source Converter (VSC) technology, on the other hand, allows for the construction of MTDC grids that support bidirectional power flows (Chaudhuri, Chaudhuri, Majumder, and Yazdani, 2014). In turn VSC HVDC based MTDC grids enable the construction of large meshed or radial DC grids such as the planned European "Supergrid", which will be capable of integrating large quantities of renewable energies over vast geographical distances (Van Hertem and Ghandhari, 2010). These grids will be capable of providing a range of ancillary services to AC networks.

As DC connections to AC grids increase there is a consequential loss in inertial response in the AC systems. To counter this, it is therefore of interest to employ frequency control to make DC connections react to frequency imbalances in a similar fashion to AC systems (Chaudhuri et al., 2014). Furthermore, allowing the DC system to react to frequency imbalances in this way decreases the necessity for additional primary and secondary frequency control reserves in AC areas connected to DC grids, as it is possible to share reserves over large distances via the DC grid (Dai, 2011). The provision of frequency control to AC areas is therefore of particular interest.

*Corresponding author.
E-mail address: paul.mcnamara@ucd.ie (P. Mc Namara).

[1] Paul Mc Namara is currently based in the Electricity Research Centre, School of Electrical, Electronic, and Communications Engineering, University College Dublin, Dublin, Ireland.

Thus far in the literature a number of different primary frequency control algorithms, which act on the milliseconds scale to counteract disturbances, have been developed (Chaudhuri, Majumder, and Chaudhuri, 2013; Dai, Phulpin, Sarlette, and Ernst, 2012; Egea-Alvarez, Bianchi, Junyent-Ferre, Gross, and Gomis-Bellmunt, 2013; Silva, Moreira, Seca, Phulpin, and Peas Lopes, 2012). By necessity these algorithms act using local information only, in a decentralised fashion, so as to be less susceptible to the effects of communication delays, as communication delays can result in instability in the primary control loop (Andreasson et al., 2013; Dai, Phulpin, Sarlette, and Ernst, 2010). Typically, these methods act by manipulating the DC voltage or current in response to the local frequency error signal.

While these primary control techniques counteract the initial effects of disturbances, it is necessary to employ some form of integral action in order to provide long term frequency regulation. Traditionally, in AC networks this has been conducted using Automatic Generation Control (AGC), which acts on the seconds to minutes scale in order to regulate frequencies. Decentralised PI based methods have been proposed recently for this purpose (Chaudhuri et al., 2014; Dai, 2011; Egea-Alvarez et al., 2015) and an optimised PID method was proposed in de Courreges d'Ustou (2012).

Transmission System Operators (TSOs) are responsible for the balancing of the electricity supply to match demand across power grids. Different sections of large power systems, such as the European grid, are controlled by separate TSOs. These TSOs conduct AGC across the interconnected grid in a decentralised fashion without using inter-TSO communication (ENTSO-E, 2004; Kundur, 1994). Two issues arise from the perspective of control design here. First of all, the poor performance of traditional decentralised PI based methods for AGC in modern power systems has been noted. The Nordic grid provides an illustrative example, where with increased penetration of renewable sources, and under traditional PI frequency control, there has been a noticeable increase in frequency violations in recent years (Ersdal, Imsland, and Uhlen, 2015). Secondly, it is well known that in highly interconnected networks decentralised control can result in highly sub-optimal performance and can potentially be a source of instability (Venkat, 2006). This decrease in performance arises as a result of ignoring the effects of interactions between interconnected areas when formulating control actions. Thus, when designing AGC for MTDC grids, optimal controllers are of interest, as well as those capable of considering the interactions between different subsystems when formulating control inputs, as a means of improving control performance.

Model Predictive Control (MPC) (Maciejowski et al., 2002) algorithms enable the optimal control of a system based on the use of state-space predictions. In recent years, there has been extensive research in the field of distributed MPC (Maestre and Negenborn, 2014). Here a number of controllers, called control agents, are responsible for the control of separate interconnected subsystems in a system, and through inter-agent communication, it is possible for them to collectively achieve a performance that approximates that of a centralised MPC controller. Additionally, in certain cases distributed MPC controllers can be shown to provide stable control in situations where equivalent communication free decentralised control causes system instability due to the presence of large interconnection coefficients between interconnected subsystems (Venkat, 2006). Distributed MPC methods have been shown to improve controller performance for AGC performance in AC networks (Kennel, Gorges, and Liu, 2013), and also in many other power systems applications (Arnold, Negenborn, Andersson, and De Schutter, 2009; Hermans et al., 2012; Ma, Chen, Liu, and Allgöwer, 2014; Moradzadeh, Boel, and Vandevelde, 2013). Previously a framework for the use of MPC for the control of MTDC grids was proposed in Mc Namara, Meere, O'Donnell, and McLoone (2015), where Centralised MPC (CMPC) and communication free decentralised Selfish MPC (SMPC) were proposed for the control of MTDC grids. Given distributed control algorithms can outperform decentralised communication free approaches, it is of interest to investigate distributed MPC for AGC in MTDC grids.

Many different schemes have been proposed for implementing distributed MPC (Maestre and Negenborn, 2014). Non-iterative schemes, where agents exchange information only once per sample step, were presented in Camponogara, Jia, Krogh, and Talukdar (2002), Liu, Chen, Muñoz de la Peña, and Christofides (2010), and Hermans, Lazar, and Jokic (2010). There are also many iterative distributed MPC methods that have been developed based on game-theoretic approaches that search for optimal equilibria (Sanchez, Giovanini, Murillo, and Limache, 2011, chap. 4; Li, Zhang, and Zhu, 2005; Zhang and Li, 2007). Other decomposition-coordination based iterative methods decompose the original control problem into several smaller optimisation problems and use communication between agents to coordinate their solutions. Examples of decomposition methods include Jacobian decomposition (Venkat, 2006), Bender's decomposition (Moroş Andan, Bourdais, Dumur, and Buisson, 2010), and the Alternating Direction Method of Multipliers (ADMOM) (Farokhi, Shames, and Johansson, 2014; Negenborn, De Schutter, and Hellendoorn, 2008).

A number of distributed MPC algorithms are based on the decomposition of a centralised augmented Lagrangian MPC formulation into subproblems which are coordinated via the updating of the dual variables (Farokhi et al., 2014; Giselsson et al., 2013; Negenborn et al., 2008). The Auxiliary Problem Principle (APP)

can be used to decompose a centralised augmented Lagrangian problem such that it can be solved in parallel via a number of subproblems in an iterative fashion (Royo, 2001). In Negenborn et al. (2008) a parallel distributed MPC method was proposed based on the APP.

Typically in power systems, for applications such as AGC, state and input constraints are not explicitly considered in control calculations. Usually an unconstrained control law is used for control, and approaches such as input saturation are used to maintain constraints (Kundur, 1994). The use of fixed feedback gains in turn allows the eigenvalues of the system to be determined, which can be used to find the system's modes of oscillation and their relationship with the various system states (assuming inputs and states are not subject to inequality constraints). It is therefore important that eigenvalue analysis techniques are developed for distributed MPC, in order to encourage their adoption in the power systems industry.

While a non-centralised control structure may be preferable for real-time control of power systems, in practice it is still typical for there to be a coordinating control layer that analyses the oscillatory modes in the system and that caters for issues such as stability and tuning. For instance, the European Network of Transmission System Operators for Electricity (ENTSO-E) is the body responsible for coordinating the actions of the various interconnected TSOs on the European electricity grid. Additionally, while control is usually conducted over short times scales, i.e., seconds to minutes, the tuning of controllers can be carried out over significantly longer periods such as hours or days. Therefore, it is reasonable to expect that modal analysis of the closed-loop system could be carried out at a central hub.

Unconstrained methods for modal analysis of distributed MPC have been developed previously (Li et al., 2005; Vaccarini et al., 2009; Zhang and Li, 2007; Zheng et al., 2013). Typically, while these techniques invoke the use of constant feedback gains coupled with centralised eigenvalue analysis, the derivation of the controllers relies on game theory or other non-Lagrangian optimisation formulations. There are several advantages to using decomposed Lagrangian techniques for distributed control. Many control practitioners are already familiar with Lagrangian optimisation theory and so would already be familiar with the theory behind the formulation of these distributed MPC approaches, which in turn would encourage the adoption of these techniques in industry. There is a large body of knowledge related to solving decentralised augmented Lagrangian problems for a range of communication topologies, thus giving practitioners much flexibility in how the control can be distributed. Additionally, significant research has been carried out to ensure efficient updating of the Lagrange multipliers, which in turn encourages an efficient implementation of the decentralised optimisation routines (Bertsekas and Tsitsikilis, 1989; Boyd and Vandenberghe, 2009; Castillo, Minguez, Conejo, and Garcia-Bertrand, 2006; Censor, 1997).

To summarise, the novel contributions of this paper are as follows:

- The application of distributed MPC for coordinating AGC in AC areas connected to MTDC grids.
- The development of a centralised eigenvalue based analysis for a closed-loop parallel Non-Cooperative distributed MPC (NCdMPC) approach, which allows for modal analysis of the MTDC system.

With regard to the modal analysis technique, the particular application here is a parallel distributed MPC technique based on the APP, but the proposed methodology can be used with any distributed MPC technique based on a decomposed augmented Lagrangian approach for eigenvalue analysis. By extension this eigenvalue analysis can be used to provide conditions for convergence and stability. The accuracy of the eigenvalue analysis is demonstrated using a 5 area Multi-Terminal HVDC (MTDC) testbed, in which AGC is implemented to share power between AC areas over the DC grid.

The remainder of the paper is organised as follows. The modelling of the AC areas and MTDC grid are given in Section 2. In Section 3 MPC is first introduced and then in Section 4 the derivation of the APP-based NCdMPC method is explained. In Section 5 the eigenvalue-based convergence and stability conditions of the algorithm are presented. The formulation of MPC for AGC in MTDC connected AC areas is described in Section 6. The technique is then tested in simulations studies on the 5 area MTDC testbed in Section 7. Conclusions and future work are presented in Section 8.

2 Modelling for multi-terminal HVDC grids

An MTDC grid is composed of a Direct Current (DC) grid and N Alternating Current (AC) areas, each with a converter that serves as an interface for transferring power to and from the DC grid, as in Fig. 1 (Sarlette, Dai, Phulpin, and Ernst, 2012). Each AC area i, for $i = 1, 2, \ldots, n$, is governed by the following

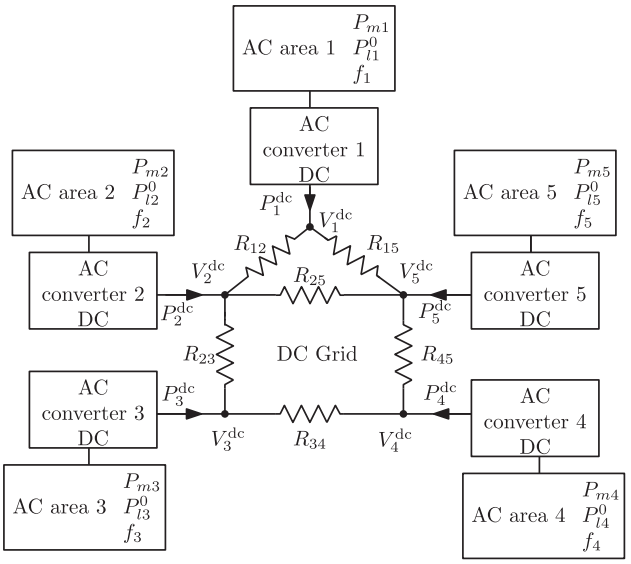

Figure 1: A multi-terminal DC grid connecting $N = 5$AC areas via converters (Sarlette et al., 2012).

dynamic equations:

$$J_i \frac{\mathrm{d}}{\mathrm{d}t} f_i(t) = \frac{P_{\mathrm{m}i}(t) - P_{\mathrm{l}i}(t) - P_i^{\mathrm{dc}}(t)}{4\pi^2 f_i(t)} - D_{gi}\left(f_i(t) - \bar{f}_i\right) \ , \tag{1}$$

$$\tau_{\mathrm{m}i} \frac{\mathrm{d}}{\mathrm{d}t} P_{\mathrm{m}i}(t) = P_{\mathrm{m}i}^0(t) - P_{\mathrm{m}i}(t) - \frac{P_{\mathrm{nom},i}}{\sigma_i} \frac{f_i(t) - \bar{f}_i}{\bar{f}_i} \ , \tag{2}$$

$$P_{\mathrm{l}i}(t) = P_{\mathrm{l}i}^0(t)\left(1 + D_{\mathrm{l}i}\left(f_i(t) - \bar{f}_i\right)\right) \ , \tag{3}$$

where J_i is the moment of inertia of aggregated area i ($\mathrm{kg\,m^2}$), $f_i(t)$ is the frequency (Hz), $P_{\mathrm{m}i}(t)$ is the mechanical power (W), $P_{\mathrm{l}i}(t)$ is the load disturbance considering frequency effects (W), $P_i^{\mathrm{dc}}(t)$ is the DC power AC area i is injecting into the DC grid (W), D_{gi} is the damping factor ($\mathrm{W\,s^2}$), $\tau_{\mathrm{m}i}$ is the time constant for power adjustment (s), $P_{\mathrm{m}i}^0(t)$ is the reference mechanical power that is manipulated using AGC (W), σ_i is the generator droop (dimensionless), $P_{li}^0(t)$ is the nominal load disturbance at bus i(W), and $D_{\mathrm{l}i}$ is the sensitivity of $P_{\mathrm{l}i}(t)$ to deviations of the frequency from the nominal operating frequency $\bar{f}_i$ (Hz^{-1} or s) (Kundur, 1994). In this paper, for a general variable b, $\bar{b}$ denotes the operating point of this variable at equilibrium, e.g., $\bar{f}_i$ denotes the nominal value of f_i. It should be noted that while this paper considers only one HVDC point of connection in each AC area, it is possible to extend the approach to the case in which there are multiple points of connection to the DC grid. This can be done by replacing the $-P_i^{\mathrm{dc}}(t)$ term in (1) with $-\sum_{j=1}^{n_{\mathrm{dci}}} P_{ij}^{\mathrm{dc}}(t)$, where P_{ij}^{dc} denotes the power injected at the j-th point of connection to the DC grid in the i-th AC area, where there are n_{dci} points of connection to the DC grid in the ith AC area.

A positive $P_i^{\mathrm{dc}}(t)$ indicates that area i is injecting P_i^{dc} W into the HVDC grid, and a negative $P_i^{\mathrm{dc}}(t)$ indicates area i is receiving P_i^{dc} W from the HVDC grid. Denoting $V_i^{\mathrm{dc}}(t)$ as the voltage at the node in the DC grid connected to AC area i, it follows that

$$P_i^{\mathrm{dc}}(t) = \sum_{j=1}^{N} \frac{V_i^{\mathrm{dc}}(t)\left(V_i^{\mathrm{dc}}(t) - V_j^{\mathrm{dc}}(t)\right)}{R_{ij}} \ , \tag{4}$$

where $R_{ij} = R_{ji}$ is the resistance in the HVDC line connecting areas i and j, and $R_{ij} = \infty$ if areas i and j are not connected by a DC line.

The voltage at the node in the DC grid connected to AC area i is manipulated as follows:

$$v_i(t) = \gamma_i x_{\mathrm{fi}}(t) + V_{\mathrm{dci}}^{\mathrm{os}}(t) \ , \tag{5}$$

where $v_i(t)$ is the DC input voltage deviation at the node in the DC grid connected to AC area i ($v_i(t) = V_i^{\mathrm{dc}}(t) - \bar{V}_i^{\mathrm{dc}}$), γ_i is the DC voltage Primary Frequency Control (PFC) gain of the i-th agent, the state $x_{fi}(t)$ is the frequency deviation of area i ($x_{fi}(t) = f_i(t) - \bar{f}_i$), and $V_{\mathrm{dci}}^{\mathrm{os}}(t)$ is a time varying voltage offset signal. The first term on the right-hand side of the equation is a PFC term that acts to alleviate the worst effects

of disturbances at a milliseconds level, using a proportional gain (Sarlette et al., 2012). As this proportional controller will result in an error offset, it is necessary to employ secondary control over longer time scales in order to eliminate these system errors over longer time periods. Thus the secondary level AGC is employed to eliminate these long term disturbances.

Here, the DC voltage (and thus the DC power) is manipulated to regulate the frequency in each AC area about a nominal DC power level. In this paper it is assumed that the dynamics of the converter and DC lines occur at time scales significantly faster than those that affect the primary and secondary frequency control of the AC system, as in Sarlette et al. (2012). Thus these faster dynamics are neglected and it is assumed that V_{dci} can be treated as an instantaneous input to the system. In reality the V_{dci} input would be sent as a setpoint to an inner loop voltage controller in the HVDC converter (Chaudhuri et al., 2014; Cole et al., 2010).

The controller in (5) operates about a nominal voltage $\bar{V}_i^{\mathrm{dc}}$. Changing the DC line power to operate about a new operating point requires the calculation of updated $\bar{V}_i^{\mathrm{dc}}$ values using a load flow calculation based on the desired DC line powers. This would be necessary, for example, in cases where power markets determine the power flows on DC grids. However, in this paper $\bar{V}_i^{\mathrm{dc}}$ is taken as constant for the duration of each simulation. It should be noted that there is a range of other well established primary DC voltage controllers, including those that explicitly consider a DC power or current setpoint; see for example Beerten, Cole, and Belmans (2014), Chaudhuri et al. (2014), and Zhang, Harnefors, and Nee (2011).

In order to control the DC voltages using MPC, $V_{\mathrm{dci}}^{\mathrm{os}}(t)$ is given the following user defined dynamic response:

$$\frac{\mathrm{d}}{\mathrm{d}t}V_{\mathrm{dci}}^{\mathrm{os}}(t) = \frac{1}{\tau_{\mathrm{dci}}}\left(V_{\mathrm{dci}}^{0}(t) - V_{\mathrm{dci}}^{\mathrm{os}}(t)\right) \ , \tag{6}$$

where $V_{dci}^{0}(t)$ is the reference signal for the secondary DC voltage offset control, and τ_{dci} is a time constant in s that is specified by the user in order to determine the speed of the response of $V_{\mathrm{dci}}^{\mathrm{os}}(t)$ (Mc Namara et al., 2015). This method of applying voltage offsets ensures that the voltages are applied to the system in a smooth manner, which is desirable both in terms of improving prediction accuracy, and avoiding sudden step jumps in the DC power delivery. The reference signals $P_{\mathrm{m}i}^{0}(t)$ and $V_{\mathrm{dci}}^{0}(t)$ are then manipulated using MPC for the purposes of AGC.

3 Model predictive control

In this section, the centralised implementation of an MPC controller is first outlined, and then in the following section the distributed APP-based MPC controller is discussed. Consider a system consisting of n non-overlapping subsystems. A discrete-time, linear, time-invariant state-space model for this system is given by

$$\mathbf{x}(k+1) = \mathbf{A}\mathbf{x}(k) + \mathbf{B}\mathbf{u}(k) \tag{7}$$

$$\mathbf{y}(k) = \mathbf{C}\mathbf{x}(k) \ , \tag{8}$$

where $\mathbf{x}(k) = \left[\mathbf{x}_1^{\mathrm{T}}(k)\dots\mathbf{x}_n^{\mathrm{T}}(k)\right]^{\mathrm{T}}$, $\mathbf{u}(k) = \left[\mathbf{u}_1^{\mathrm{T}}(k)\dots\mathbf{u}_m^{\mathrm{T}}(k)\right]^{\mathrm{T}}$, $\mathbf{y}(k) = \left[\mathbf{y}_1^{\mathrm{T}}(k)\dots\mathbf{y}_p^{\mathrm{T}}(k)\right]^{\mathrm{T}}$, and $\mathbf{x}_a(k)$, $\mathbf{u}_a(k)$, and $\mathbf{y}_a(k)$ are the states, inputs, and outputs of subsystem a at sample step k, respectively. Matrices $\mathbf{A}$, $\mathbf{B}$, and $\mathbf{C}$ are the relevant state-space matrices. An incremental state space model is used for control in order to ensure integral action:

$$\mathbf{x}^{\mathrm{aug}}(k+1) = \hat{\mathbf{A}}\mathbf{x}^{\mathrm{aug}}(k) + \hat{\mathbf{B}}\Delta\mathbf{u}(k) \ , \tag{9}$$

$$\mathbf{y}(k+1) = \hat{\mathbf{C}}\mathbf{x}^{\mathrm{aug}}(k+1) \ , \tag{10}$$

where $\Delta\mathbf{p}(k) = \mathbf{p}(k) - \mathbf{p}(k-1)$ for a general vector $\mathbf{p}$, $\mathbf{x}^{\mathrm{aug}}(k) = \left[\Delta\mathbf{x}^{\mathrm{T}}(k)\mathbf{x}^{\mathrm{T}}(k)\right]^{\mathrm{T}}$ is the augmented state vector, and $\hat{\mathbf{A}}$, $\hat{\mathbf{B}}$, and $\hat{\mathbf{C}}$ are the incremental state-space matrices.

To simplify notation, the prediction vector, over a horizon H is first introduced. For a general vector $\mathbf{p}$, its prediction vector is $\tilde{\mathbf{p}}(k) = \left[\mathbf{p}^{\mathrm{T}}(k)\dots\mathbf{p}^{\mathrm{T}}(k+H-1)\right]^{\mathrm{T}}$. State and output predictions over the prediction horizon are then determined as follows:

$$\tilde{\mathbf{x}}^{\mathrm{aug}}(k+1) = \hat{\mathbf{A}}^{\mathrm{f}}\mathbf{x}^{\mathrm{aug}}(k) + \hat{\mathbf{B}}^{\mathrm{f}}\Delta\tilde{\mathbf{u}}(k) \tag{11}$$

$$\tilde{\mathbf{y}}^{\mathrm{aug}}(k+1) = \hat{\mathbf{C}}^{\mathrm{f}}\tilde{\mathbf{x}}^{\mathrm{aug}}(k+1) \ , \tag{12}$$

where $\hat{\mathbf{A}}^{\mathrm{f}}$, $\hat{\mathbf{B}}^{\mathrm{f}}$, and $\hat{\mathbf{C}}^{\mathrm{f}}$ are the state-space prediction matrices. The derivation of these matrices is well established in the literature (Maciejowski et al., 2002).

MPC problems are constructed to fulfil control objectives for a system based on knowledge of $\mathbf{x}(k)$. A cost function, $J(\mathbf{x}(k), \Delta\tilde{\mathbf{u}}(k))$ (where $J(k)$ will be used henceforth for compactness), is designed so as to embody the system's objectives. Typically this cost function is chosen to be a quadratic function in terms of $\Delta\tilde{\mathbf{u}}$ and in this paper the cost function takes the following form:

$$J(k) = \tilde{\mathbf{e}}^{\mathrm{T}}\mathbf{Q}_{\mathrm{e}}\tilde{\mathbf{e}} + \Delta\tilde{\mathbf{u}}^{\mathrm{T}}\mathbf{Q}_{\mathrm{u}}\Delta\tilde{\mathbf{u}} \ , \tag{13}$$

where the $(k+1)$ dependency is dropped from $\tilde{\mathbf{e}}(k+1)$, and the (k) dependency is dropped from $\Delta\tilde{\mathbf{u}}(k)$ in (13) for compactness, the error vector, $\mathbf{e}(k) = \left[\mathbf{e}_1^{\mathrm{T}}(k) \dots \mathbf{e}_n^{\mathrm{T}}(k)\right]^{\mathrm{T}}$, where $\mathbf{e}_a(k) = \mathbf{y}_a(k) - \mathbf{r}_a(k)$, and $\mathbf{r}_a(k)$ are the reference signals of subsystem a at sample step k. The weighting matrices $\mathbf{Q}_{\mathrm{e}}$ and $\mathbf{Q}_{\mathrm{u}}$ determine the relative importance of minimising errors, the incremental changes in states, and the incremental changes in inputs, respectively.

The centralised MPC problem that is solved at each sample step is then given by

$$\Delta\tilde{\mathbf{u}}(k) = \min_{\Delta\tilde{\mathbf{u}}(k)\in\mathcal{U}} J(k) \ , \tag{14}$$

where $\mathcal{U}$ defines the set of constraints for $\Delta\tilde{\mathbf{u}}(k)$. Here only $\Delta\mathbf{u}(k)$ is applied to the system, and the optimisation process is conducted at each sample step.

As discussed in the Introduction, centralised implementations of AGC may not be feasible given the traditionally decentralised structure of frequency control. To circumvent these issues, MPC can be performed in a distributed fashion, allowing individual areas the autonomy to perform AGC locally, while coordinating their responses with other interconnected subsystems. The distributed MPC approach used in this paper is described in the next section.

4 Distributed MPC

The distributed MPC method will now be described and the links between this approach and the centralised MPC approach will be discussed. The centralised state-space model, given by (7) and (8), is expressed in its equivalent distributed form by

$$\mathbf{x}_a(k+1) = \mathbf{A}_a\mathbf{x}_a(k) + \mathbf{B}_a\mathbf{u}_a(k) + \mathbf{V}_a\mathbf{v}_a(k) \tag{15}$$

$$\mathbf{y}_a(k) = \mathbf{C}_a\mathbf{x}_a(k) \ , \tag{16}$$

where $\mathbf{x}_a(k)$ are the states of subsystem a, $\mathbf{u}_a(k)$ are subsystem inputs, $\mathbf{y}_a(k)$ are subsystem outputs, and $\mathbf{v}_a(k)$ are external inputs from other subsystems that influence subsystem a at sample step k, for $a = 1, \dots, n$. The matrices $\mathbf{A}_a$, $\mathbf{B}_a$, $\mathbf{V}_a$, and $\mathbf{C}_a$ are the relevant state-space matrices.

It should be noted here that the external input variables $\mathbf{v}_a$ are a modelling necessity from a distributed modelling point of view. From a centralised MPC modelling perspective the variables $\mathbf{v}_a$ are simply a subset of the centralised state vector $\mathbf{x}$, originating from some subsystems $j \neq a$, that influence the states $\mathbf{x}_a$. Thus these variables serve as means of representing the interconnection between the states of subsystem a and the states of other subsystems.

An incremental state-space model is used for control in order to ensure integral action:

$$\mathbf{x}_a^{\mathrm{aug}}(k+1) = \hat{\mathbf{A}}_a\mathbf{x}_a^{\mathrm{aug}}(k) + \hat{\mathbf{B}}_a\Delta\mathbf{u}_a(k) + \hat{\mathbf{V}}_a\Delta\mathbf{v}_a(k) \tag{17}$$

$$\mathbf{y}_a(k+1) = \hat{\mathbf{C}}_a\mathbf{x}_a^{\mathrm{aug}}(k+1) \ , \tag{18}$$

where $\mathbf{x}_a^{\mathrm{aug}}(k) = \left[\Delta\mathbf{x}_a^{\mathrm{T}}(k)\mathbf{x}_a^{\mathrm{T}}(k)\right]^{\mathrm{T}}$ is the augmented state vector of the a-th subsystem, and $\hat{\mathbf{A}}_a$, $\hat{\mathbf{B}}_a$, $\hat{\mathbf{V}}_a$, and $\hat{\mathbf{C}}_a$ are the incremental state space matrices for subsystem a.

State and output predictions for subsystem a over the prediction horizon are then determined using (17) and (18) as follows:

$$\tilde{\mathbf{x}}_a^{\mathrm{aug}}(k+1) = \hat{\mathbf{A}}_a^{\mathrm{f}}\mathbf{x}_a^{\mathrm{aug}}(k) + \hat{\mathbf{B}}_a^{\mathrm{f}}\Delta\tilde{\mathbf{u}}_a(k) + \hat{\mathbf{V}}_a^{\mathrm{f}}\Delta\tilde{\mathbf{v}}_a(k) \tag{19}$$

$$\tilde{\mathbf{y}}_a^{\mathrm{aug}}(k) = \hat{\mathbf{C}}_a^{\mathrm{f}}\tilde{\mathbf{x}}_a^{\mathrm{aug}}(k) \ , \tag{20}$$

where $\hat{\mathbf{A}}_a^{\mathrm{f}}$, $\hat{\mathbf{B}}_a^{\mathrm{f}}$, $\hat{\mathbf{V}}_a^{\mathrm{f}}$, and $\hat{\mathbf{C}}_a^{\mathrm{f}}$ are the incremental state-space prediction matrices, derived using the same techniques for state space prediction as in the centralised case.

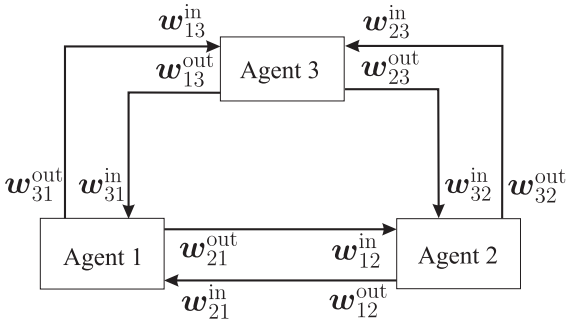

Figure 2: Interconnecting inputs and outputs for 3 connected subsystems.

Non-cooperative distributed MPC based on the APP, which was originally devised in Negenborn et al. (2008), is now described. This is formed first by deriving a centralised augmented Lagrangian formulation of the MPC problem in terms of the distributed state-space representation of the system given by (17) and (18). Having shown how this centralised augmented Lagrangian problem would be solved, it is then illustrated how this problem is decomposed into subproblems using the APP, which in turn can be solved in parallel in a distributed fashion.

Let agent $j \in \mathcal{N}_a$ be connected to agent a, where $\mathcal{N}_a$ is the set of agents connected to agent a by a common variable, and $a \notin \mathcal{N}_a$. The interconnecting input vector, $\mathbf{w}_{ja}^{\text{in}}$, is defined as the vector of inputs to control problem a from agent $j \in \mathcal{N}_a^{\text{in}}$, where $\mathcal{N}_a^{\text{in}} \subseteq \mathcal{N}_a$ is the ordered set of agents connected to agent a by an interconnecting input. Likewise, the interconnecting output vector $\mathbf{w}_{ja}^{\text{out}}$ is defined as the vector of outputs to control problem $j \in \mathcal{N}_a^{\text{out}}$ from agent a, where $\mathcal{N}_a^{\text{out}} \subseteq \mathcal{N}_a$ is the ordered set of agents connected to agent a by an interconnecting output. As an illustration, interconnecting inputs and outputs for a 3 agent system are shown in Fig. 2.

The vector of all interconnecting inputs $\mathbf{w}_a^{\text{in}}(k)$, and all interconnecting outputs $\mathbf{w}_a^{\text{out}}(k)$ of the control problem of agent a are typically defined as follows:

$$\begin{aligned}\mathbf{w}_a^{\text{in}}(k) &= \left[\mathbf{w}_{\mathcal{N}_a^{\text{in}}\{1\}a}^{\text{inT}}(k) \ \dots \ \mathbf{w}_{\mathcal{N}_a^{\text{in}}\{m_a\}a}^{\text{inT}}(k)\right]^{\text{T}} = \mathbf{v}_a(k) \ , \\ \mathbf{w}_a^{\text{out}}(k) &= \left[\mathbf{w}_{\mathcal{N}_a^{\text{out}}\{1\}a}^{\text{out}}(k) \ \dots \ \mathbf{w}_{\mathcal{N}_a^{\text{out}}\{q_a\}a}^{\text{outT}}(k)\right]^{\text{T}} = \mathbf{K}_a^{\text{out}}\mathbf{x}_a(k) \ ,\end{aligned} \tag{21}$$

where $\mathcal{N}_a^{\text{in}}\{i\}$ denotes the i-th element of $\mathcal{N}_a^{\text{in}}$, and $\mathcal{N}_a^{\text{out}}\{i\}$ denotes the i-th element of $\mathcal{N}_a^{\text{out}}$. There are m_a agents connected to agent a by an interconnecting input, q_a agents are connected to agent a by an interconnecting output, and $\mathbf{K}_a^{\text{out}}$ is a matrix of zeros and ones, used to select the states in $\mathbf{x}_a(k)$ that connect agent a to other subnetworks.

For a system of n subsystems, the overall MPC problem can be stated as follows:

$$\boldsymbol{\theta}^*(k) = \arg\min_{\boldsymbol{\theta}(k)} \sum_{a=1}^{n} J_a^{\text{local}}(k) \ , \tag{22}$$

subject to the following equality constraints over the prediction horizon:

$$\tilde{\mathbf{w}}_{ja}^{\text{in}}(k+1) = \tilde{\mathbf{w}}_{aj}^{\text{out}}(k+1), \quad \forall j \in \mathcal{N}_a, \ \forall a \in \{1, \dots, n\} \ , \tag{23}$$

where $\boldsymbol{\theta}(k) = \left[\Delta\tilde{\mathbf{u}}^{\text{T}}(k), \Delta\tilde{\mathbf{w}}^{\text{inT}}(k+1)\right]^{\text{T}}$, with $\Delta\tilde{\mathbf{u}}(k) = \left[\Delta\tilde{\mathbf{u}}_1^{\text{T}}(k), \dots, \Delta\tilde{\mathbf{u}}_n^{\text{T}}(k)\right]^{\text{T}}$, $\Delta\tilde{\mathbf{w}}^{\text{in}}(k) = \left[\Delta\tilde{\mathbf{w}}_1^{\text{inT}}(k), \dots, \Delta\tilde{\mathbf{w}}_n^{\text{inT}}(k)\right]^{\text{T}}$, and $J_a^{\text{local}}(k)$ represents the local control goals for subsystem a. The vector $\tilde{\mathbf{w}}_{aj}^{\text{out}}(k+1)$ is dependent on $\Delta\tilde{\mathbf{u}}_j(k)$ and $\tilde{\mathbf{w}}_j^{\text{in}}(k)$ as follows:

$$\tilde{\mathbf{w}}_{aj}^{\text{out}}(k+1) = \mathbf{K}_{aj}\left(\hat{\mathbf{A}}_j^{\text{f}}\mathbf{x}_j^{\text{aug}}(k) + \hat{\mathbf{B}}_j^{\text{f}}\Delta\tilde{\mathbf{u}}_j(k) + \hat{\mathbf{V}}_j^{\text{f}}\Delta\tilde{\mathbf{w}}_j^{\text{in}}(k)\right) \tag{24}$$

where $\mathbf{K}_{aj}$ is a matrix of zeros, with entries of 1 such that the equality (24) holds.

It should be noted here that variables $\Delta\tilde{\mathbf{w}}^{\text{in}}(k+1)$ are added to the optimisation problem as duplicate variables of the interconnecting flows between subproblems. These allow a subsystem to optimise the value of the interconnecting flows that it would like to receive from connected subsystems over the prediction horizon. Equality constraint (23) ensures that the interconnecting flows between areas over the prediction horizon

are equal, which has the effect of improving the overall control performance of the system. Furthermore, it is the addition of these local variables to the optimisation problem that allows the optimisation problem to be distributed amongst the individual subproblems once the APP is applied.

An augmented Lagrangian formulation can be derived from (22) to incorporate the equality constraints (23) into the cost function. Augmented Lagrangian formulations iteratively solve, first, a primal problem and then update the dual variables related to the active constraints. The primal centralised problem solved at each augmented Lagrangian iteration l, for sample step k, is given as follows:

$$\boldsymbol{\theta}^*(k,l) = \arg\min_{\boldsymbol{\theta}(k)} \sum_{a=1}^{n} \Bigg(J_a^{\text{local}}(k,l) + \sum_{j\in N_a} \Big(\tilde{\boldsymbol{\lambda}}_{ja}^{\text{inT}}(k+1,l) \left(\tilde{\mathbf{w}}_{ja}^{\text{in}}(k+1,l) - \tilde{\mathbf{w}}_{aj}^{\text{out}}(k+1,l) \right) + \frac{c}{2} \left\| \tilde{\mathbf{w}}_{ja}^{\text{in}}(k+1,l) - \tilde{\mathbf{w}}_{aj}^{\text{out}}(k+1,l) \right\|_2^2 \Big) \Bigg) \tag{25}$$

where $\tilde{\boldsymbol{\lambda}}_{ja}^{\text{in}}(k+1,l)$ is the vector of Lagrange multipliers associated with the equality constraints placed on the variables connecting agents a and j over the prediction horizon, at augmented Lagrangian iteration l and sample step k.

In this paper, $J_a^{\text{local}}(k,l)$ is given by

$$J_a^{\text{local}}(k,l) = \tilde{\mathbf{e}}_a^{\text{T}}(k+1,l)\mathbf{Q}_a\tilde{\mathbf{e}}_a(k+1,l) + \Delta\tilde{\mathbf{u}}_a^{\text{T}}(k,l)\mathbf{R}_a\Delta\tilde{\mathbf{u}}_a(k,l) \tag{26}$$

where $\mathbf{Q}_a$ and $\mathbf{R}_a$ are agent a's local MPC weights, and $\mathbf{e}_a(k+1,l) = \mathbf{y}_a(k+1,l) - \mathbf{r}_a(k+1)$ is the vector of predicted tracking errors in the MPC problem at iteration l of the distributed MPC cycle for sample step $k+1$, where $\mathbf{y}_a(k+1,l)$ are subsystem a's outputs and $\mathbf{r}_a(k+1)$ is a vector of subsystem a's reference signals.

After solving (25), the Lagrange multipliers are updated as follows for iteration $l+1$:

$$\tilde{\boldsymbol{\lambda}}_{ja}^{\text{in}}(l+1) = \tilde{\boldsymbol{\lambda}}_{ja}^{\text{in}}(l) + c\left(\tilde{\mathbf{w}}_{ja}^{\text{in}}(l) - \tilde{\mathbf{w}}_{aj}^{\text{out}}(l)\right) \quad , \tag{27}$$

where the $(k+1)$ dependency is dropped from all variables above for compactness. The following is then conducted in an iterative fashion; (25) is first solved, followed by the updating of the Lagrange multipliers, as in (27). This process is repeated until the following termination condition is met:

$$\left\| \tilde{\boldsymbol{\lambda}}_{ja}^{\text{in}}(k+1,l+1) - \tilde{\boldsymbol{\lambda}}_{ja}^{\text{in}}(k+1,l) \right\|_\infty \leq \epsilon \quad \forall j \in \mathcal{N}_a,\ \forall a \in \{1,\ldots,n\} \ , \tag{28}$$

where ϵ is a small tolerance and $\|\cdot\|_\infty$ denotes the infinity norm. The infinity norm is used here so that the Lagrange multipliers of all interconnecting inputs agree within a specified tolerance. It should be noted that the centralised formulation presented here is formed in the same way as in Negenborn et al. (2008), but in the current paper the only constraints that are explicitly considered are the equality constraints placed on the interconnecting variables.

Problem (25) is distributed across the agents using the Auxiliary Problem Principle (Royo, 2001). The APP works by allowing agents to solve an approximation of the centralised augmented Lagrangian problem in a parallel fashion. As the APP is closely related to the ADMOM, it is shown first how the ADMOM distributes the solving of augmented Lagrangians exactly. Then it can be seen that the APP is very similar to the ADMOM in formulation, with the main difference being the addition of an extra quadratic term which encourages convergence between iterations and allows the problem to be solved in parallel. Further details on the relationship between the ADMOM and APP can be found in Royo (2001).

Take the optimisation problem:

$$\begin{aligned} \mathbf{x} = \left[\mathbf{x}_1^{\text{T}}, \mathbf{x}_2^{\text{T}}\right]^{\text{T}} &= \arg\min_{\mathbf{x}_1,\mathbf{x}_2} \left(f_1(\mathbf{x}_1) + f_2(\mathbf{x}_2)\right) \\ &\text{such that } \mathbf{x}_1 = \mathbf{x}_2 \ . \end{aligned} \tag{29}$$

The unconstrained augmented Lagrangian form of this equation at iteration l of the augmented Lagrangian optimisation is given as

$$\mathbf{x}(l) = \arg\min_{\mathbf{x}_1,\mathbf{x}_2} f_1(\mathbf{x}_1(l)) + f_2(\mathbf{x}_2(l)) + \boldsymbol{\lambda}^{\text{T}}(l)\left(\mathbf{x}_1(l) - \mathbf{x}_2(l)\right) + \frac{c}{2}\left\|\mathbf{x}_1(l) - \mathbf{x}_2(l)\right\|_2^2 \tag{30}$$

where $\mathbf{x}(l) = \left[\mathbf{x}_1^{\text{T}}(l), \mathbf{x}_2^{\text{T}}(l)\right]^{\text{T}}$, $\boldsymbol{\lambda}(l)$ are the Lagrange multipliers at iteration l of the augmented Lagrangian optimisation. Using the ADMOM (30) is solved in a serial fashion for iteration l of the augmented Lagrangian

optimisation as follows:

$$\begin{aligned}\mathbf{x}_1(l) &= \arg\min_{\mathbf{x}_1(l)} \; f_1\left(\mathbf{x}_1(l)\right) + \boldsymbol{\lambda}^{\mathrm{T}}(l)\mathbf{x}_1(l) + \frac{c}{2}\left\|\mathbf{x}_1(l) - \mathbf{x}_2(l-1)\right\|_2^2 \\ \mathbf{x}_2(l) &= \arg\min_{\mathbf{x}_2(l)} \; f_2\left(\mathbf{x}_2(l)\right) - \boldsymbol{\lambda}^{\mathrm{T}}(l)\mathbf{x}_2(l) + \frac{c}{2}\left\|\mathbf{x}_1(l) - \mathbf{x}_2(l)\right\|_2^2 \;\; . \end{aligned} \tag{31}$$

In the above each subproblem solves for its local variables keeping the most recent updates of variables from the connected subproblem constant. Afterwards each subproblem then communicates its optimised variable value to the connected subproblem. The second quadratic term in the objective function seeks to achieve consensus on the value of the variables connecting the two subproblems.

The APP has a similar structure in its final form to the ADMOM, where it solves the primal augmented Lagrangian problem in a parallel distributed fashion as follows:

$$\begin{aligned}\mathbf{x}_1(l) &= \arg\min_{\mathbf{x}_1(l)} \; f_1\left(\mathbf{x}_1(l)\right) + \boldsymbol{\lambda}^{\mathrm{T}}(l)\mathbf{x}_1(l) + \frac{c}{2}\left\|\mathbf{x}_1(l) - \mathbf{x}_2(l-1)\right\|_2^2 + \frac{b-c}{2}\left\|\mathbf{x}_1(l) - \mathbf{x}_1(l-1)\right\|_2^2 \\ \mathbf{x}_2(l) &= \arg\min_{\mathbf{x}_2(l)} \; f_2\left(\mathbf{x}_2(l)\right) - \boldsymbol{\lambda}^{\mathrm{T}}(l)\mathbf{x}_2(l) + \frac{c}{2}\left\|\mathbf{x}_2(l) - \mathbf{x}_1(l-1)\right\|_2^2 + \frac{b-c}{2}\left\|\mathbf{x}_2(l) - \mathbf{x}_2(l-1)\right\|_2^2 \end{aligned} \tag{32}$$

where $b \geq 2c$. It can be seen that the APP now adds a third quadratic cost to the objective function which encourages subproblems at iteration l to converge on the value for their local interconnecting variables based on the value from iteration $l-1$.

Thus applying the APP to solve the primal augmented Lagrangian MPC problem (30), the optimisation problem of agent a, for iteration l of the distributed MPC cycle, at sample step k is

$$\boldsymbol{\theta}_a^*(k,l) = \arg\min_{\boldsymbol{\theta}_a(k,l)} \; \left(J_a^{\mathrm{local}}(k,l) + J_a^{\mathrm{inter}}(k,l)\right) \;\; , \tag{33}$$

where $\boldsymbol{\theta}_a(k,l) = \left[\Delta\tilde{\mathbf{u}}_a^{\mathrm{T}}(k,l), \Delta\tilde{\mathbf{w}}_a^{\mathrm{inT}}(k+1,l)\right]^{\mathrm{T}}$.

The interconnecting cost for agent a, $J_a^{\mathrm{inter}}(k,l)$, is given by

$$J_a^{\mathrm{inter}}(k,l) = \sum_{j \in N_a} J_{ja}^{\mathrm{inter}}(k,l) \;\; , \tag{34}$$

and $J_{ja}^{\mathrm{inter}}(k,l)$ is the cost associated with the inter-agent coordination with agent j given by

$$\begin{aligned} J_{ja}^{\mathrm{inter}}(k,l) = &\begin{bmatrix} \tilde{\boldsymbol{\lambda}}_{ja}^{\mathrm{in}}(k+1,l) \\ -\tilde{\boldsymbol{\lambda}}_{aj}^{\mathrm{in}}(k+1,l) \end{bmatrix}^{\mathrm{T}} \begin{bmatrix} \tilde{\mathbf{w}}_{ja}^{\mathrm{in}}(k+1,l) \\ \tilde{\mathbf{w}}_{ja}^{\mathrm{out}}(k+1,l) \end{bmatrix} + \frac{c}{2}\left\| \begin{bmatrix} \tilde{\mathbf{w}}_{ja}^{\mathrm{out}}(k+1,l) - \tilde{\mathbf{w}}_{aj}^{\mathrm{in}}(k+1,l-1) \\ \tilde{\mathbf{w}}_{ja}^{\mathrm{in}}(k+1,l) - \tilde{\mathbf{w}}_{aj}^{\mathrm{out}}(k+1,l-1) \end{bmatrix} \right\|_2^2 \\ &+ \frac{b-c}{2}\left\| \begin{bmatrix} \tilde{\mathbf{w}}_{ja}^{\mathrm{out}}(k+1,l) - \tilde{\mathbf{w}}_{ja}^{\mathrm{out}}(k+1,l-1) \\ \tilde{\mathbf{w}}_{ja}^{\mathrm{in}}(k+1,l) - \tilde{\mathbf{w}}_{ja}^{\mathrm{in}}(k+1,l-1) \end{bmatrix} \right\|_2^2 \;\; . \end{aligned} \tag{35}$$

As mentioned previously, it is useful, in power systems, to be able to determine the oscillatory modes of the closed-loop system under NCdMPC. In the next section it will be shown how these modes can be found.

5 Modal analysis of non-cooperative distributed MPC including convergence and stability conditions

As the APP results in a decomposition of the centralised MPC problem given in (25), the closed-loop modes that would be given by using (25), will be equal to the modes of operation of the system under NCdMPC using the APP (or any other Lagrangian decomposition technique). Thus a closed-loop expression is derived for (25), in order to analyse the behaviour of the system under NCdMPC.

Firstly, it is desired to derive the optimal value of $\boldsymbol{\theta}(k,l)$ at iteration l and sample step k of the centralised augmented Lagrangian problem (25). Thus in the following paragraphs (25) is expressed in matrix form and manipulated so as to express (25) as a quadratic optimisation problem. The interconnecting inputs and outputs and the Lagrange multipliers are grouped into the terms $\tilde{\mathbf{w}}^{\mathrm{in}}(k,l)$, $\tilde{\mathbf{w}}^{\mathrm{out}}(k,l)$, and $\tilde{\boldsymbol{\lambda}}(k+1,l)$,

respectively, where

$$\tilde{\mathbf{w}}^{\text{in}}(k,l) = \begin{bmatrix} \tilde{\mathbf{w}}^{\text{in}}_{\mathcal{N}_1^{\text{in}}\{1\}1}(k,l) \\ \tilde{\mathbf{w}}^{\text{in}}_{\mathcal{N}_1^{\text{in}}\{2\}1}(k,l) \\ \vdots \\ \tilde{\mathbf{w}}^{\text{in}}_{\mathcal{N}_1^{\text{in}}\{m_1\}1}(k,l) \\ \cdots \ \cdots \\ \vdots \\ \cdots \ \cdots \\ \tilde{\mathbf{w}}^{\text{in}}_{\mathcal{N}_n^{\text{in}}\{1\}n}(k,l) \\ \tilde{\mathbf{w}}^{\text{in}}_{\mathcal{N}_n^{\text{in}}\{2\}n}(k,l) \\ \vdots \\ \tilde{\mathbf{w}}_{\mathcal{N}_n^{\text{in}}\{m_n\}n}(k,l) \end{bmatrix} , \tag{36}$$

$$\tilde{\mathbf{w}}^{\text{out}}(k,l) = \begin{bmatrix} \tilde{\mathbf{w}}^{\text{out}}_{\mathcal{N}_1^{\text{out}}\{1\}1}(k,l) \\ \tilde{\mathbf{w}}^{\text{out}}_{\mathcal{N}_1^{\text{out}}\{2\}1}(k,l) \\ \vdots \\ \tilde{\mathbf{w}}^{\text{out}}_{\mathcal{N}_1^{\text{out}}\{q_1\}1}(k,l) \\ \cdots \ \cdots \\ \vdots \\ \cdots \ \cdots \\ \tilde{\mathbf{w}}^{\text{out}}_{\mathcal{N}_n^{\text{out}}\{1\}n}(k,l) \\ \tilde{\mathbf{w}}^{\text{out}}_{\mathcal{N}_n^{\text{out}}\{2\}n}(k,l) \\ \vdots \\ \tilde{\mathbf{w}}^{\text{out}}_{\mathcal{N}_n^{\text{out}}\{q_n\}n}(k,l) \end{bmatrix} , \tag{37}$$

$$\tilde{\boldsymbol{\lambda}}(k+1,l) = \begin{bmatrix} \tilde{\boldsymbol{\lambda}}^{\text{in}}_{\mathcal{N}_1^{\text{in}}\{1\}1}(k+1,l) \\ \tilde{\boldsymbol{\lambda}}^{\text{in}}_{\mathcal{N}_1^{\text{in}}\{2\}1}(k+1,l) \\ \vdots \\ \tilde{\boldsymbol{\lambda}}^{\text{in}}_{\mathcal{N}_1^{\text{in}}\{m_1\}1}(k+1,l) \\ \cdots \ \cdots \\ \vdots \\ \cdots \ \cdots \\ \tilde{\boldsymbol{\lambda}}^{\text{in}}_{\mathcal{N}_n^{\text{in}}\{1\}n}(k+1,l) \\ \tilde{\boldsymbol{\lambda}}^{\text{in}}_{\mathcal{N}_n^{\text{in}}\{2\}n}(k+1,l) \\ \vdots \\ \tilde{\boldsymbol{\lambda}}^{\text{in}}_{\mathcal{N}_n^{\text{in}}\{m_n\}n}(k+1,l) \end{bmatrix} , \tag{38}$$

where agent a has m_a interconnecting inputs and q_a interconnecting outputs.

The term $J^{\text{local}}(k,l)$ is used to represent the sum of the local cost functions in (25), i.e.,

$$J^{\text{local}}(k,l) = \sum_{a=1}^{n} J_a^{\text{local}}(k,l) \ . \tag{39}$$

Using the incremental prediction models (19) and (20), $J^{\text{local}}(k,l)$ is represented using the various system variables as follows:

$$J^{\text{local}}(k,l) = \tilde{\mathbf{e}}^{\text{T}}(k+1,l)\mathbf{Q}\tilde{\mathbf{e}}(k+1,l) + \Delta\tilde{\mathbf{u}}^{\text{T}}(k,l)\mathbf{R}\Delta\tilde{\mathbf{u}}(k,l) \ , \tag{40}$$

where $\tilde{\mathbf{e}}(k+1,l) = \tilde{\mathbf{y}}(k+1,l) - \tilde{\mathbf{r}}(k+1)$, with outputs $\mathbf{y}(k) = \left[\mathbf{y}_1^{\mathrm{T}}(k), \mathbf{y}_2^{\mathrm{T}}(k), \ldots, \mathbf{y}_n^{\mathrm{T}}(k)\right]^{\mathrm{T}}$, setpoints $\tilde{\mathbf{r}}(k) = \left[\tilde{\mathbf{r}}_1^{\mathrm{T}}(k), \ldots, \tilde{\mathbf{r}}_n^{\mathrm{T}}(k)\right]^{\mathrm{T}}$, $\mathbf{Q} = \mathrm{diag}\left(\mathbf{Q}_1, \ldots, \mathbf{Q}_n\right)$, $\mathbf{R} = \mathrm{diag}\left(\mathbf{R}_1, \ldots, \mathbf{R}_n\right)$, and $\tilde{\mathbf{y}}(k+1,l) = \mathbf{K}_{\mathrm{c}}\tilde{\boldsymbol{\chi}}^{\mathrm{aug}}\ (k+1,l) = \mathbf{K}_{\mathrm{c}}\left(\hat{\mathbf{A}}^{\mathrm{f}}\mathbf{x}^{\mathrm{aug}}(k) + \hat{\mathbf{B}}^{\mathrm{f}}\Delta\tilde{\mathbf{u}}(k,l) + \hat{\mathbf{V}}^{\mathrm{f}}\left[\Delta\mathbf{v}^{\mathrm{T}}(k), \Delta\tilde{\mathbf{w}}^{\mathrm{inT}}(k+1,l)\right]^{\mathrm{T}}\right.$. The state of the entire system is $\mathbf{x}^{\mathrm{aug}}(k) = \left[\mathbf{x}_1^{\mathrm{augT}}(k), \ldots, \mathbf{x}_n^{\mathrm{aug\ T}}(k)\right]^{\mathrm{T}}$, the system's predicted incremental inputs $\Delta\tilde{\mathbf{u}}(k,l) = \left[\Delta\tilde{\mathbf{u}}_1^{\mathrm{T}}(k,l), \ldots, \Delta\tilde{\mathbf{u}}_n^{\mathrm{T}}(k,l)\right]^{\mathrm{T}}$, the vector $\Delta\mathbf{v}(k) = \left[\Delta\mathbf{v}_1^{\mathrm{T}}(k), \ldots, \Delta\mathbf{v}_n^{\mathrm{T}}(k)\right]^{\mathrm{T}}$ is a column vector of the incremental changes in the different subsystems' interconnecting inputs at sample step k, and $\Delta\tilde{\mathbf{w}}^{\mathrm{in}}(k+1,l) = \left[\Delta\tilde{\mathbf{w}}_1^{\mathrm{inT}}(k+1,l), \ldots, \Delta\tilde{\mathbf{w}}_n^{\mathrm{inT}}(k+1,l)\right]^{\mathrm{T}}$ is a column vector of the incremental changes in the predicted interconnecting inputs of each subsystem over the prediction horizon, and their associated prediction matrices are given by $\hat{\mathbf{A}}^{\mathrm{f}} = \mathrm{diag}\left(\hat{\mathbf{A}}_1^{\mathrm{f}}, \ldots, \hat{\mathbf{A}}_n^{\mathrm{f}}\right)$, $\hat{\mathbf{B}}^{\mathrm{f}} = \mathrm{diag}\left(\hat{\mathbf{B}}_1^{\mathrm{f}}, \ldots, \hat{\mathbf{B}}_n^{\mathrm{f}}\right)$, and $\hat{\mathbf{V}}^{\mathrm{f}} = \mathrm{diag}\left(\hat{\mathbf{V}}_1^{\mathrm{f}}, \ldots, \hat{\mathbf{V}}_n^{\mathrm{f}}\right)$. Here, $\mathbf{K}_{\mathrm{c}}$ is a matrix of zeros and ones, with entries of 1 in the positions that select the outputs $\tilde{\mathbf{y}}(k+1,l)$ from the augmented state prediction vector $\tilde{\mathbf{x}}^{\mathrm{aug}}(k+1,l)$.

Let $\tilde{\mathbf{y}}(k+1,\mathbf{l}) = \mathbf{K}_{\mathrm{c}}\mathbf{D}\mathbf{s}(k) + \mathbf{K}_{\mathrm{c}}\mathbf{Z}\boldsymbol{\theta}(k,l)$, with $\mathbf{D} = \left[\hat{\mathbf{A}}^{\mathrm{f}}, \hat{\mathbf{V}}_{\mathrm{v}}^{\mathrm{f}}\right]$ and vector $\mathbf{s}(k) = \left[\mathbf{x}^{\mathrm{augT}}(k), \Delta\mathbf{v}^{\mathrm{T}}(k)\right]^{\mathrm{T}}$. Given the matrix $\hat{\mathbf{V}}^{\mathrm{f}} = \left[\mathbf{V}_{\mathrm{V}}^{\mathrm{f}}, \hat{\mathbf{V}}_{\mathrm{w}^{\mathrm{in}}}^{\mathrm{f}}\right]$, the matrix $\hat{\mathbf{V}}_{\mathrm{v}}^{\mathrm{f}}$ determines the effect of $\Delta\mathbf{v}(k)$ on $\tilde{\mathbf{x}}^{\mathrm{aug}}(k+1,l)$. The matrix $\hat{\mathbf{V}}_{\mathrm{w}}^{\mathrm{f}}$ in similarly determines the effect of $\Delta\tilde{\mathbf{w}}^{\mathrm{in}}(k+1,l)$ on $\tilde{\mathbf{x}}^{\mathrm{aug}}(k+1,l)$. Note that $\mathbf{K}_{\mathrm{c}}\mathbf{D}\mathbf{s}(k)$ is fixed during the MPC iterations at each sample step. The latter group of terms $\mathbf{K}_{\mathrm{c}}\mathbf{Z}\boldsymbol{\theta}(k,l)$ varies, via the manipulation of $\boldsymbol{\theta}(k,l)$, where $\mathbf{Z} = \left[\hat{\mathbf{B}}^{\mathrm{f}}, \hat{\mathbf{V}}_{\mathrm{w}^{\mathrm{in}}}^{\mathrm{f}}\right]$.

The interconnecting inputs are given by $\tilde{\mathbf{w}}^{\mathrm{in}}(k,l) = \mathbf{K}_{\mathrm{v}}\mathbf{s}(k) + \mathbf{K}_{\mathrm{w}}\boldsymbol{\theta}(k,l)$ where $\mathbf{K}_{\mathrm{v}}$ is used to select the relevant interconnecting variables from $\mathbf{s}(k)$, and $\mathbf{K}_{\mathrm{w}}$ selects the relevant incremental interconnecting inputs from $\boldsymbol{\theta}(k,l)$. The interconnecting outputs are given by $\tilde{\mathbf{w}}^{\mathrm{out}}(k,l) = \mathbf{K}_{\mathrm{I}}(\mathbf{D}\mathbf{s}(k) + \mathbf{Z}\boldsymbol{\theta}(k,l))$, where $\mathbf{K}_{\mathrm{I}}$ is used to pick out the relevant outputs. The term $\tilde{\mathbf{w}}^{\mathrm{in}}(k,l) - \tilde{\mathbf{w}}^{\mathrm{out}}(k,l)$ which is used when seeking equality on all pairs of interconnecting inputs and outputs is now given by

$$\begin{aligned}\tilde{\mathbf{w}}^{\mathrm{in}}(k,l) - \tilde{\mathbf{w}}^{\mathrm{out}}(k,l) &= \mathbf{K}_{\mathrm{v}}\mathbf{s}(k) + \mathbf{K}_{\mathrm{w}}\boldsymbol{\theta}(k,l) - \mathbf{K}_{\mathrm{l}}(\mathbf{D}\mathbf{s}(k) + \mathbf{Z}\boldsymbol{\theta}(k,l)) \\ &= \left(\mathbf{K}_{\mathrm{v}} - \mathbf{K}_{\mathrm{l}}\mathbf{D}\right)\mathbf{s}(k) + \left(\mathbf{K}_{\mathrm{w}} - \mathbf{K}_{\mathrm{l}}\mathbf{Z}\right)\boldsymbol{\theta}(k,l) \\ &= \mathbf{K}_{\mathrm{s}}\mathbf{s}(k) + \mathbf{K}_{\theta}\boldsymbol{\theta}(k,l)\end{aligned}$$

where $\mathbf{K}_{\mathrm{s}} = \mathbf{K}_{\mathrm{v}} - \mathbf{K}_{\mathrm{l}}\mathbf{D}$ and $\mathbf{K}_{\theta} = \mathbf{K}_{\mathrm{w}} - \mathbf{K}_{\mathrm{l}}\mathbf{Z}$.

Problem (25) can now be stated as

$$\begin{aligned}\boldsymbol{\theta}^*(k,l) = \arg\min_{\boldsymbol{\theta}(k,l)}\ &\mathbf{E}^{\mathrm{T}}\mathbf{Q}\mathbf{E} + \boldsymbol{\theta}^{\mathrm{T}}(k,l)\mathbf{R}_{\theta}\boldsymbol{\theta}(k,l) \\ &+ \tilde{\boldsymbol{\lambda}}^{\mathrm{T}}(k+1,l)\left(\mathbf{K}_{\mathrm{s}}\mathbf{s}(k) + \mathbf{K}_{\theta}\boldsymbol{\theta}(k,l)\right) \\ &+ \frac{c}{2}\left(\mathbf{K}_{\mathrm{s}}\mathbf{s}(k) + \mathbf{K}_{\theta}\boldsymbol{\theta}(k,l)\right)^{\mathrm{T}}\left(\mathbf{K}_{\mathrm{s}}\mathbf{s}(k) + \mathbf{K}_{\theta}\boldsymbol{\theta}(k,l)\right)\end{aligned} \tag{41}$$

where $\mathbf{E} = (\mathbf{P}\mathbf{s}(k) + \mathbf{G}\boldsymbol{\theta}(k,l) - \tilde{\mathbf{r}}(k+1))$, $\mathbf{P} = \mathbf{K}_{\mathrm{c}}\mathbf{D}$, $\mathbf{G} = \mathbf{K}_{\mathrm{c}}\mathbf{Z}$, and $\mathbf{R}_{\theta} = \mathrm{diag}\left(\mathbf{R}, \mathbf{0}_{(N-1)n_v \times (N-1)n_v}\right)$ with n_v being the size of $\mathbf{v}$.

With some matrix manipulation, it is possible to represent (41) in the following quadratic form:

$$\boldsymbol{\theta}^*(k,l) = \arg\min_{\boldsymbol{\theta}(k,l)} J^{\mathrm{quad}}(k,l) = \arg\min_{\boldsymbol{\theta}(k,l)} \boldsymbol{\theta}^{\mathrm{T}}(k,l)\mathbf{H}\boldsymbol{\theta}(k,l) + \boldsymbol{\theta}^{\mathrm{T}}(k,l)\mathbf{f}(k,l) + \vartheta(k)\ . \tag{42}$$

Here,

$$\mathbf{H} = \mathbf{G}^{\mathrm{T}}\mathbf{Q}\mathbf{G} + \mathbf{R}_{\theta} + \frac{c}{2}\mathbf{K}_{\theta}^{\mathrm{T}}\mathbf{K}_{\theta}\ , \tag{43}$$

$$\mathbf{f}(k,l) = 2\mathbf{G}^{\mathrm{T}}\mathbf{Q}\mathbf{P}\mathbf{s}(k) - 2\mathbf{G}^{\mathrm{T}}\mathbf{Q}\tilde{\mathbf{r}}(k+1) + \mathbf{K}_{\theta}^{\mathrm{T}}\tilde{\boldsymbol{\lambda}}(k+1,l) + c\mathbf{K}_{\theta}^{\mathrm{T}}\mathbf{K}_{s}\mathbf{s}(k)\ , \tag{44}$$

$$\begin{aligned}\vartheta(k) = {}&\mathbf{s}^{\mathrm{T}}(k)\mathbf{P}^{\mathrm{T}}\mathbf{Q}\mathbf{P}\mathbf{s}(k) - 2\tilde{\mathbf{r}}^{\mathrm{T}}(k+1)\mathbf{Q}\mathbf{P}\mathbf{s}(k) + \tilde{\boldsymbol{\lambda}}^{\mathrm{T}}(k+1,l)\mathbf{K}_{\mathrm{s}}\mathbf{s}(k) \\ &+ \frac{c}{2}\mathbf{s}^{\mathrm{T}}(k)\mathbf{K}_{\mathrm{s}}^{\mathrm{T}}\mathbf{K}_{\mathrm{s}}\mathbf{s}(k) + \tilde{\mathbf{r}}^{\mathrm{T}}(k+1)\mathbf{Q}\tilde{\mathbf{r}}(k+1)\end{aligned} \tag{45}$$

where $\vartheta(k)$ is a scalar that does not depend on $\boldsymbol{\theta}(k,l)$.

The value of $\boldsymbol{\theta}^*(k,l)$ at sample step k and iteration l of the centralised augmented Lagrangian problem is found by setting $\frac{\partial}{\partial\theta(k,l)}J^{\mathrm{quad}}(k,l) = 0$, which yields

$$\boldsymbol{\theta}^*(k,l) = -\frac{1}{2}\mathbf{H}^{-1}\mathbf{f}(k,l)\ , \tag{46}$$

where $\mathbf{H}$ is a positive definite.

After $\boldsymbol{\theta}^*(k,l)$ is found, the Lagrange multipliers are calculated as follows:

$$\begin{aligned}\tilde{\boldsymbol{\lambda}}(k+1,l+1) &= \tilde{\boldsymbol{\lambda}}(k+1,l) + c\left(\tilde{\mathbf{w}}^{\text{in}}(k,l) - \tilde{\mathbf{w}}^{\text{out}}(k,l)\right)\\ &= \tilde{\boldsymbol{\lambda}}(k+1,l) + c\left(\mathbf{K}_{\text{s}}\mathbf{s}(k) + \mathbf{K}_\theta\boldsymbol{\theta}^*(k,l)\right)\\ &= \tilde{\boldsymbol{\lambda}}(k+1,l) + c\mathbf{K}_s\mathbf{s}(k) - \frac{c}{2}\mathbf{K}_\theta\mathbf{H}^{-1}\left(2\mathbf{G}^{\text{T}}\mathbf{Q}\mathbf{P}\mathbf{s}(k) - 2\mathbf{G}^{\text{T}}\mathbf{Q}\tilde{\mathbf{r}}(k+1)\right.\\ &\quad \left. + \mathbf{K}_\theta^{\text{T}}\tilde{\boldsymbol{\lambda}}(k+1,l) + c\mathbf{K}_\theta^{\text{T}}\mathbf{K}_{\text{s}}\mathbf{s}(k)\right)\\ &= \left(\mathrm{I}_{n_\lambda\times n_\lambda} - \frac{c}{2}\mathbf{K}_\theta\mathbf{H}^{-1}\mathbf{K}_\theta^{\text{T}}\right)\tilde{\boldsymbol{\lambda}}(k+1,l) + \mathbf{C}_\lambda(k)\end{aligned} \tag{47}$$

where n_λ is the length of vector $\tilde{\boldsymbol{\lambda}}(k+1,l)$, and $\mathbf{C}_\lambda(k) = c\mathbf{K}_s\mathbf{s}(k) - \frac{1}{2}c\mathbf{K}_\theta\mathbf{H}^{-1}\big(2\mathbf{G}^{\text{T}}\mathbf{Q}(\mathbf{P}\mathbf{s}(k) - \tilde{\mathbf{r}}(k+1)) + c\mathbf{K}_\theta^{\text{T}}\mathbf{K}_s\mathbf{s}(k)\big)$ is a constant over the course of the optimisation at sample step k.

The vector of eigenvalues related to the convergence of the NCdMPC algorithm is then given by

$$\boldsymbol{\rho}_{\text{c}} = \text{eig}\left(\mathrm{I}_{n_\lambda\times n_\lambda} - \frac{c}{2}\mathbf{K}_\theta\mathbf{H}^{-1}\mathbf{K}_\theta^{\text{T}}\right) \ , \tag{48}$$

where $\mathbf{K}_\theta\mathbf{H}^{-1}\mathbf{K}_\theta^{\text{T}}$ is non-singular. The convergence condition for the NCdMPC algorithm is then

$$\|\rho_c\|_\infty < 1 \ . \tag{49}$$

Upon convergence of the augmented Lagrangian iterations $\tilde{\boldsymbol{\lambda}}(k+1,l+1) \to \tilde{\boldsymbol{\lambda}}(k+1,l) = \tilde{\boldsymbol{\lambda}}^*(k+1)$, where $\tilde{\boldsymbol{\lambda}}^*(k+1)$ is the optimal Lagrange multiplier vector at sample step k. Eq. (47) then yields

$$\begin{aligned}\tilde{\boldsymbol{\lambda}}^*(k+1) &= \left(\mathrm{I}_{n_\lambda\times n_\lambda} - \frac{c}{2}\mathbf{K}_\theta\mathbf{H}^{-1}\mathbf{K}_\theta^{\text{T}}\right)\tilde{\boldsymbol{\lambda}}^*(k+1) + \mathbf{C}_\lambda(k)\\ \tilde{\boldsymbol{\lambda}}^*(k+1) &= \frac{2}{c}\left(\mathbf{K}_\theta\mathbf{H}^{-1}\mathbf{K}_\theta^{\text{T}}\right)^{-1}\mathbf{C}_\lambda(k) \ .\end{aligned} \tag{50}$$

Substituting $\tilde{\boldsymbol{\lambda}}^*(k+1)$ back into (46) and rearranging the matrices gives

$$\boldsymbol{\theta}^*(k) = -\frac{1}{2}\mathbf{H}^{-1}\mathbf{f}(k,l) = \mathbf{F}\tilde{\mathbf{r}}(k+1) - \mathbf{W}\mathbf{s}(k) \tag{51}$$

where

$$\mathbf{F} = -\mathbf{H}^{-1}\left(\mathbf{K}_\theta^{\text{T}}\left(\mathbf{K}_\theta\mathbf{H}^{-1}\mathbf{K}_\theta^{\text{T}}\right)^{-1}\mathbf{K}_\theta\mathbf{H}^{-1}\mathbf{G}^{\text{T}}\mathbf{Q} - \mathbf{G}^{\text{T}}\mathbf{Q}\right) \ , \tag{52}$$

$$\begin{aligned}\mathbf{W} = -\mathbf{H}^{-1}\Big(&\mathbf{K}_\theta^{\text{T}}\left(\mathbf{K}_\theta\mathbf{H}^{-1}\mathbf{K}_\theta^{\text{T}}\right)^{-1}\mathbf{K}_\theta\mathbf{H}^{-1}\mathbf{G}^{\text{T}}\mathbf{Q}\mathbf{P} - \mathbf{G}^{\text{T}}\mathbf{Q}\mathbf{P} - \frac{c}{2}\mathbf{K}_\theta^{\text{T}}\mathbf{K}_s\\ &-\mathbf{K}_\theta^{\text{T}}\left(\mathbf{K}_\theta\mathbf{H}^{-1}\mathbf{K}_\theta^{\text{T}}\right)^{-1}\mathbf{K}_s + \frac{c}{2}\mathbf{K}_\theta^{\text{T}}\left(\mathbf{K}_\theta\mathbf{H}^{-1}\mathbf{K}_\theta^{\text{T}}\right)^{-1}\mathbf{K}_\theta\mathbf{H}^{-1}\mathbf{K}_\theta^{\text{T}}\mathbf{K}_s\Big) \ .\end{aligned} \tag{53}$$

At this stage it is noted that the interconnecting input variables $\Delta\mathbf{v}(k)$ are simply a subset of $\mathbf{x}^{\text{aug}}(k)$. Thus the following is used to express $\mathbf{s}(k)$ in terms of $\mathbf{x}^{\text{aug}}(k)$ for the purpose of deriving closed-loop equations in terms of $\mathbf{x}^{\text{aug}}(k)$:

$$\mathbf{s}(k) = \begin{bmatrix}\mathbf{x}^{\text{aug}}(k)\\ \Delta\mathbf{v}(k)\end{bmatrix} = \begin{bmatrix}\mathrm{I}_{n_x\times n_x}\\ \mathbf{L}\end{bmatrix}\mathbf{x}^{\text{aug}}(k) = \mathbf{r}\mathbf{x}^{\text{aug}}(k) \ , \tag{54}$$

where the matrix L selects $\Delta\mathbf{v}(k)$ from $\mathbf{x}^{\text{aug}}(k)$.

The optimal input applied to the system is

$$\Delta\mathbf{u}^*(k) = \mathbf{S}\boldsymbol{\theta}^*(k) \ , \tag{55}$$

where $\mathbf{S}$ selects the optimal system inputs at sample step k from $\boldsymbol{\theta}^*(k)$.

The discrete-time state-space equation for the whole system is then

$$\begin{aligned}\mathbf{x}^{\text{aug}}(k+1) &= \mathbf{D}\mathbf{s}(k) + \mathbf{B}\Delta\mathbf{u}^*(k)\\ &= (\mathbf{D}\boldsymbol{\Upsilon} - \mathbf{Z}\mathbf{S}\mathbf{W}\mathbf{Y})\mathbf{x}^{\text{aug}}(k) + \mathbf{B}\mathbf{S}\mathbf{F}\tilde{\mathbf{r}}(k+1)\end{aligned} \tag{56}$$

The vector of the closed-loop eigenvalues of the system under NCdMPC, ρ_s, is given by

$$\boldsymbol{\rho}_{\mathrm{s}} = \mathrm{eig}(\mathbf{D\Upsilon} - \mathbf{ZSWY}) \ , \tag{57}$$

and the conditions for the closed-loop stability of the system are then given by

$$\|\rho_s\|_\infty < 1 \ . \tag{58}$$

Using (50) and (58) it is possible to tune the distributed MPC controller in order to ensure that the agents converge on a final decision each sample step, and that the control itself is stable. Additionally, analysis of the closed-loop eigenvalues of the system using (57) can allow practitioners to determine what the closed-loop modes of oscillation will be in the system under closed-loop distributed MPC.

6 MPC formulation for AGC in MTDC connected AC systems

A methodology similar to that given in Mc Namara et al. (2015) for the application of MPC to AGC in MTDC connected AC systems is used in this paper. To avoid the significant increase in communication overhead that would arise from having to share DC power measurement information between AC areas, here, instead the DC powers are estimated from the frequencies and voltage offsets. This is described in the following. The objective function for area i at sample step k, $\Psi_i(k)$, is given by

$$\Psi_i(k) = Q_{\mathrm{fi}} x_{\mathrm{fi}}^2(k+1) + R_{\mathrm{P}i}\Delta u_{\mathrm{P}i}^2(k) + R_{\mathrm{vi}}\Delta u_{\mathrm{v}i}^2(k) \ , \tag{59}$$

where $u_{\mathrm{P}i}(k) = P_{\mathrm{m}i}^0(k) - \bar{P}_{\mathrm{m}i}^0$ and $u_{\mathrm{v}i}(k) = V_{\mathrm{dc}i}^0(k) - \bar{V}_{\mathrm{dc}i}^0$. The parameters Q_{fi}, $R_{\mathrm{P}i}$, and R_{vi} are weights that determine the relative importance of minimising $x_{\mathrm{fi}}^2(k+1)$, $\Delta u_{\mathrm{Pi}}^2(k)$, and $\Delta u_{\mathrm{vi}}^2(k)$, respectively. The first 3 terms in (59) are concerned with fulfilling the power system objectives of minimising the weighted sum of the frequency deviations about $\bar{f}_i$, the mechanical power offset control effort, and the DC voltage offset control effort, respectively.

In order to develop a linear model for use in state-space prediction, it is necessary to linearise equations (1) and (4), in order to generate state predictions. These linearisations are given as follows, as in Dai (2011):

$$\frac{\mathrm{d}}{\mathrm{d}t} f_i(t) = \frac{P_{\mathrm{m}i}(t) - P_{\mathrm{l}i}(t) - P_i^{\mathrm{dc}}(t)}{4\pi^2 \bar{f}_i J_i} - \frac{D_{\mathrm{g}i}}{J_i}\left(f_i(t) - \bar{f}_i\right) \tag{60}$$

$$\begin{aligned} z_i(t) &= \sum_{j=1}^{N} \frac{\bar{V}_i^{\mathrm{dc}}\left(v_i(t) - v_j(t)\right)}{R_{ij}} \\ &= \sum_{j=1}^{N} \frac{\bar{V}_i^{\mathrm{dc}}\left(V_{\mathrm{dc}i}^{\mathrm{os}}(t) + \gamma_i x_{\mathrm{fi}i}(t) - \left(V_{\mathrm{dcj}}^{\mathrm{os}}(t) + \gamma_j x_{\mathrm{fj}}(t)\right)\right)}{R_{ij}} \end{aligned} \tag{61}$$

where $z_i(t) = P_i^{\mathrm{dc}}(t) - \bar{P}_i^{\mathrm{dc}}$.

The state-space equations (2), (6), and (60) are then used to describe the dynamics of the system about an operating point where the state of agent i is given by $\mathbf{x}_i = [x_{\mathrm{f}i}, x_{\mathrm{P}i}, x_{\mathrm{v}i}]^{\mathrm{T}}$. Here, $x_{\mathrm{P}i} = P_{\mathrm{m}i}(t) - \bar{P}_{\mathrm{m}i}$ and $x_{\mathrm{v}ii} = V_{\mathrm{dc}i}^{\mathrm{os}}(t) - \bar{V}_{\mathrm{dc}i}^{\mathrm{os}}$ are the mechanical power and DC voltage deviations about the operating point, respectively. Agents are assumed to be capable of communicating with other agents if the AC areas they control are connected via a HVDC line. The interconnecting inputs to agent i are given by $\mathbf{w}_{ji}^{\mathrm{in}} = [x_{\mathrm{fj}}, x_{\mathrm{vj}}]^{\mathrm{T}}$, for $j \in \mathcal{N}_i$.

The input to agent i is given by $\mathbf{u}_i = [u_{\mathrm{P}i}, u_{\mathrm{v}ii}]^{\mathrm{T}}$, and its output by $y_i = \mathbf{C}_i\mathbf{x}_i$, where $\mathbf{C}_i = [1, 0, 0]$. The matrices $\mathbf{A}_i$, $\mathbf{B}_i$, and $\mathbf{V}_i$ can then be constructed as in (15), using (2), (6), and (60). In turn the state space can be framed in terms of incremental inputs $\Delta\mathbf{u}_i = [\Delta u_{\mathrm{P}i}, \Delta u_{\mathrm{vi}}]^{\mathrm{T}}$, as in (17) and (18), and the state-space predictions can then be made using (19) and (20). Each subsystem is then allocated its own control agent. Using state-space predictions each agent generates a local cost function:

$$J_i^{\mathrm{local}}(k) = \sum_{p=k}^{k+H-1} \Psi_i(p) \ . \tag{62}$$

This cost function can be described in matrix form as in (26), where $\mathbf{Q}_i = \mathrm{diag}\left(\mathbf{Q}_{ii}, \ldots, \mathbf{Q}_{ii}\right)$, $\mathbf{R}_i = \mathrm{diag}\left(\mathbf{R}_{ii}, \ldots, \mathbf{R}_{ii}\right)$, $\mathbf{Q}_{ii} = \mathrm{diag}\left(0, 0, 0, Q_{\mathrm{fi}}, 0, 0\right)$, and $\mathbf{R}_{ii} = \mathrm{diag}\left(R_{\mathrm{P}i}, R_{\mathrm{vi}}\right)$. To form the interconnection cost

Table 1: AC and DC grid parameters (Dai, 2011).

AC grid parameters					
Area	1	2	3	4	5
f_{nom} (Hz)	50	50	50	50	50
P_{m}^0 (MW)	50	80	50	30	80
P_{nom} (MW)	50	80	50	30	80
J ($\text{kg}\,\text{m}^2$)	2026	6485	6078	2432	4863
D_g ($\text{W}\,\text{s}^2$)	48.4	146.3	140	54.9	95.1
T_{sm} (s)	1.5	2.0	2.5	2	1.8
P_1^0 (MW)	100.42	59.58	40.31	49.70	39.59
D_l (Hz^{-1})	0.01	0.01	0.01	0.01	0.01
$\bar{V}^{\text{dc}}$ (kV)	99.17	99.6	99.73	99.59	100
$\bar{P}^{\text{dc}}$ (MW)	-50.4	20	10	-20	40.4
σ (no units)	0.02	0.04	0.06	0.04	0.03
γ ($\text{kV}\,\text{Hz}^{-1}$)	1	1	1	1	1
τ_{m} (s)	1.5	2	2.5	2	1.8
DC grid resistances (Ω)					
R_{12}					
1.39	4.17	2.78	6.95	2.78	2.78

(34), first variables $\tilde{\mathbf{w}}_{ij}^{\text{in}}(k+1,l-1)$ and $\tilde{\mathbf{w}}_{ij}^{\text{out}}(k+1,l-1)$ must be received from each agent i connected to agent j and the other variables in (34) are then formed as described in Section 4.

As this paper does not consider inequality constraints when solving the MPC algorithms it is possible to solve for the distributed MPC problem through the use of fixed feedback gains. This is achieved by solving

$$\frac{\text{d}}{\text{d}\boldsymbol{\theta}_i(k,l)} J_i^{\text{local}}(k,l) + J_i^{\text{inter}}(k,l) = 0 \tag{63}$$

which gives $\theta_i^*(k,l)$ once solved.

7 Experiment on a multi-terminal HVDC system

In this section NCdMPC is used to distribute AGC between AC areas connected to an MTDC grid. The modal analysis derived in the paper is also employed to analyse the system.

7.1 Simulation setup

Simulations were carried out on a testbed, previously developed in Dai (2011), to evaluate the accuracy of the modal analysis algorithm. The testbed for simulations was the 5 agent testbed given in Fig. 1. The frequencies in the AC areas in this testbed are very sensitive to load deviations, which makes it a useful benchmark problem for evaluating frequency control algorithms. It is also an interesting testbed from the perspective of parameter tuning as the system becomes unstable for certain combinations of MPC weights; hence it serves as an illustrative example of the utility of the eigenvalue analysis for predicting instability in the system, as will be presented in the results. The simulations were carried using a per unit conversion with base power $S_{\text{base}} = 100$ MW, base voltage $V_{\text{base}} = 100$ kV, and base frequency $f_{\text{base}} = 50$ Hz, using the parameter values for the AC and DC grids given in Table 1. All simulations were conducted using Matlab and Simulink.

A number of simulations were carried out for various values of $R_{\text{P}i}$, as this parameter has a significant impact on the position of the closed-loop poles of the system. For these simulations $Q_{fi} = 1$, $R_{\text{v}i} = 5, c = 1, b = 2$, and $\epsilon = 10^{-6}$. A sample step of 0.1 s and a prediction horizon of $H = 10$ was used for the controller. The sets that define the agents that communicate to coordinate their responses are given as

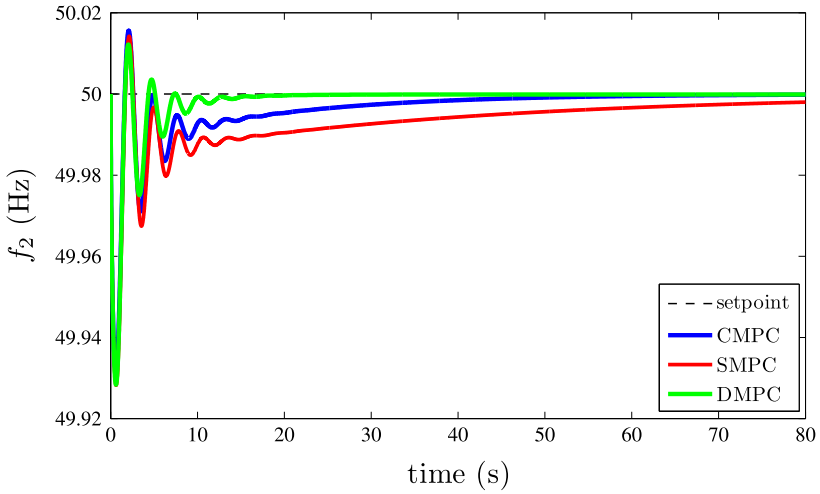

Figure 3: Plot of the frequencies in each area when SMPC, CMPC, and NCdMPC controllers are used.

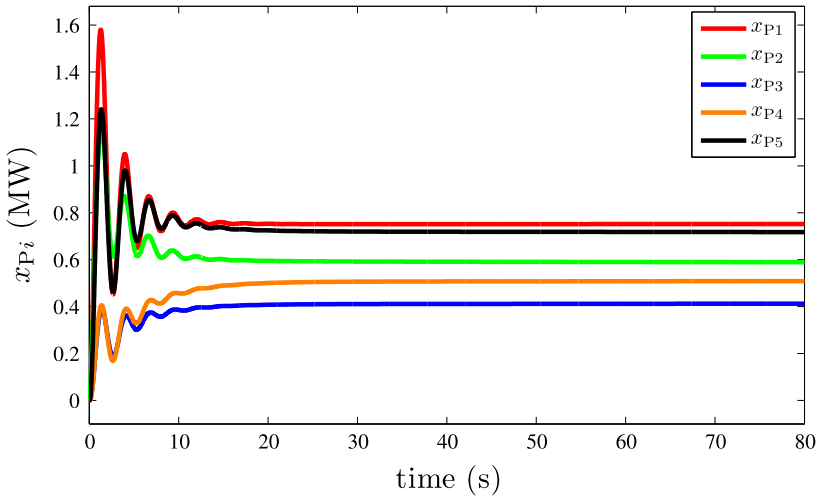

Figure 4: Plot of the mechanical power deviations from their starting values when NCdMPC is used.

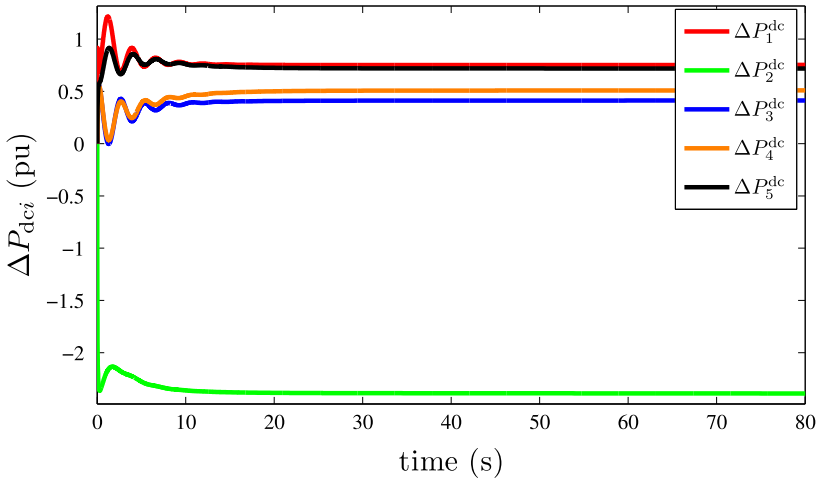

Figure 5: Plot of the DC powers deviations about their starting values in each area when NCdMPC is used.

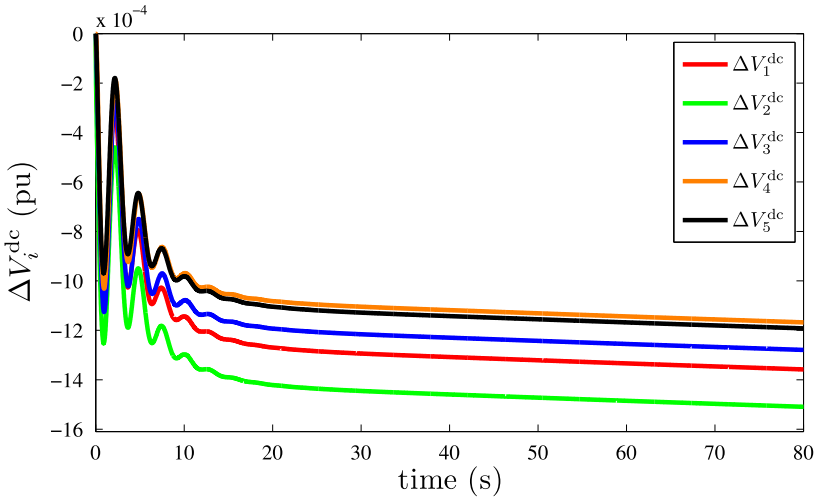

Figure 6: Plot of the DC voltage deviations about their starting values in each area when NCdMPC is used.

follows: $\mathcal{N}_1 = \{2, 5\}$, $\mathcal{N}_2 = \{1, 3, 5\}$, $\mathcal{N}_3 = \{2, 4\}$, $\mathcal{N}_4 = \{3, 5\}$, and $\mathcal{N}_5 = \{1, 2, 4\}$. In each of the simulations the system was excited by a 5% increase in P_{12}^0 which is sufficient to determine whether the dominant modes in the system are accurately determined by the method developed in this paper. In the first simulation the NCdMPC controller is compared to a CMPC and an SMPC controller. The equivalent state-space modelling and tuning used for the NCdMPC controller are used for the CMPC and SMPC controllers. The CMPC and SMPC controllers are similar to those derived previously in Mc Namara et al. (2015) for the control of the 5 area MTDC grid testbed, and use the same state-space structure as presented in Section 6.

The nonlinear system was simulated in discrete time with a sample step of $t_s = 0.01$ s using dynamics equations (1), (2), (3), (4), (5), and (6). Agents did not have access to disturbance measurements and so the controllers had to compensate for the unknown step disturbance and nonlinearities. It was assumed that measurements were noise free, that the system states were fully observable, and that a high speed communication network is in place to allow communication between the control agents that are connected via a DC line, and between the control agents and their local actuators.

7.2 Results

Plots of the frequencies, mechanical powers, DC powers, and DC voltages from each AC area, taken from the nonlinear simulation, are given in Figs. 3–6, respectively, for $R_{Pi} = 0.1$. Fig. 3 shows a comparison of the frequency responses of the NCdMPC controller and the equivalent SMPC and CMPC controllers. It can be seen that the NCdMPC controller here supplies the fastest frequency setpoint tracking after the initial disturbance in comparison to the CMPC and SMPC controller. The SMPC controller gives the worst frequency setpoint tracking performance of the 3 controllers, taking the longest time to return the frequency to its original setpoint.

Figs. 4 and 5 show the mechanical and DC power reactions when the system is under NCdMPC. It can be seen that area 2 uses the power generated in other areas, particularly that generated in areas 1 and 5 , in order to regulate its frequency, demonstrating the cooperative nature of frequency regulation across the DC grid. It is typically desirable that DC voltages do not experience large deviations from their nominal positions. It can be seen in Fig. 6 that the DC voltages remain near their nominal positions, and so the frequency regulation here does not appear to adversely affect the DC voltage regulation.

Then two more simulations were run for $R_{\mathrm{P}i} = 10^{-6}$ and $R_{\mathrm{P}i} = 10^{-7}$, in order to demonstrate the accuracy with which the NCdMPC modal analysis predicts the modes of oscillation of the system. Plots of the frequencies against time from the nonlinear system simulation, and the corresponding positions of the discrete-time eigenvalues, found from the linearised model, are given in Figs. 7–9, for $R_{\mathrm{P}i} = 10^{-6}$, 10^{-7} and 0.1 , respectively, where Fig. 9 provides a closer look at the first 10 s of the simulation for $R_{\mathrm{P}_i} = 0.1$. Figs. 7 and 8 are illustrative in terms of showing the accuracy with which the eigenvalues can be used here to predict instability in the system. In Fig. 7 it can be seen that as the largest eigenvalues approach the unit circle, the resultant response is highly oscillatory but stable. With a very small adjustment to $R_{\mathrm{P}i} = 10^{-7}$, the system is seen to go unstable and this is predicted by the corresponding eigenvalues, which lie outside of the unit circle, as can be seen in Fig. 8.

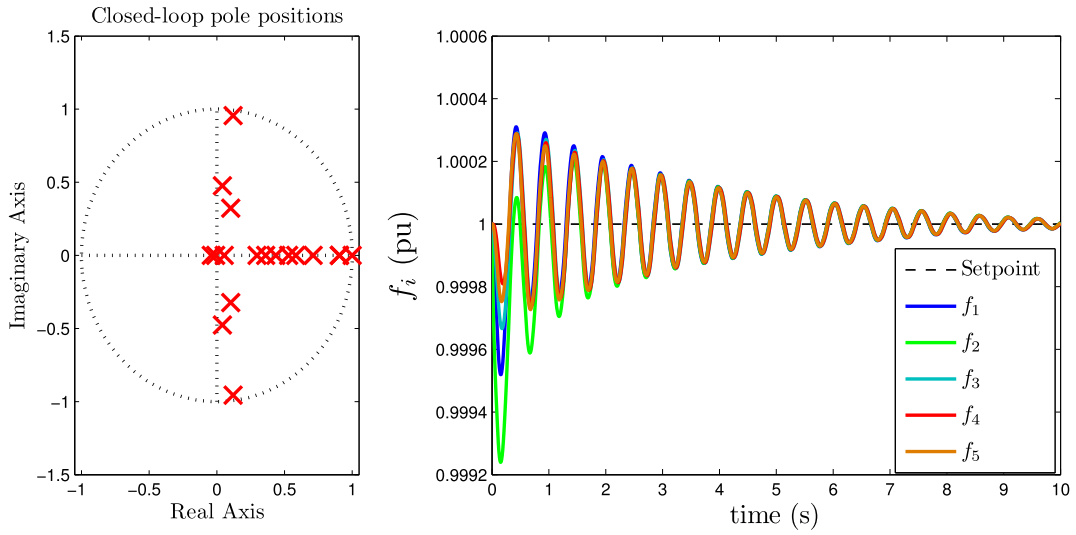

Figure 7: Plot of discrete-time poles and corresponding frequency response for $R_{Pi} = 10^{-6}$.

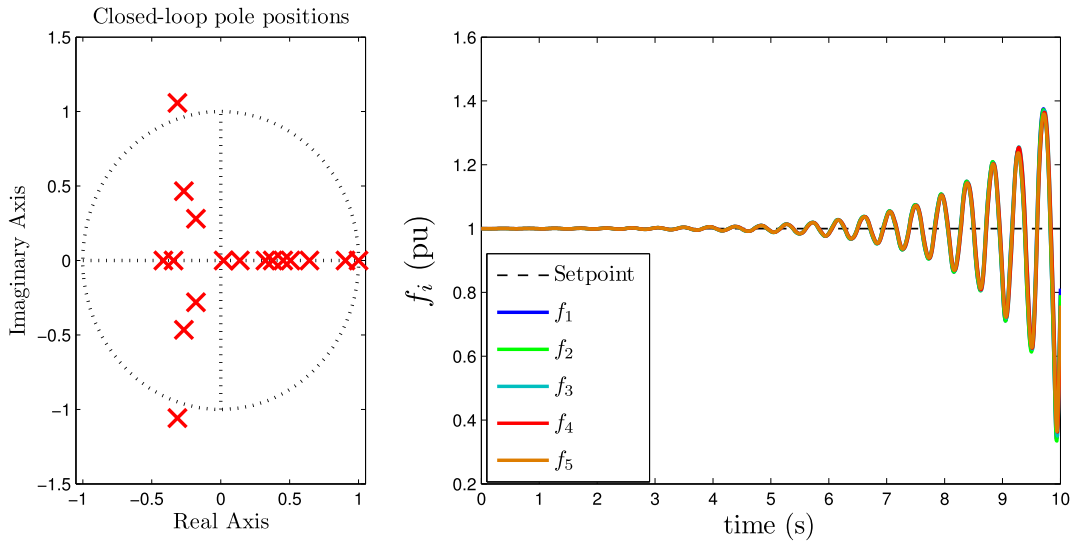

Figure 8: Plot of discrete-time poles and corresponding frequency response for $R_{Pi} = 10^{-7}$.

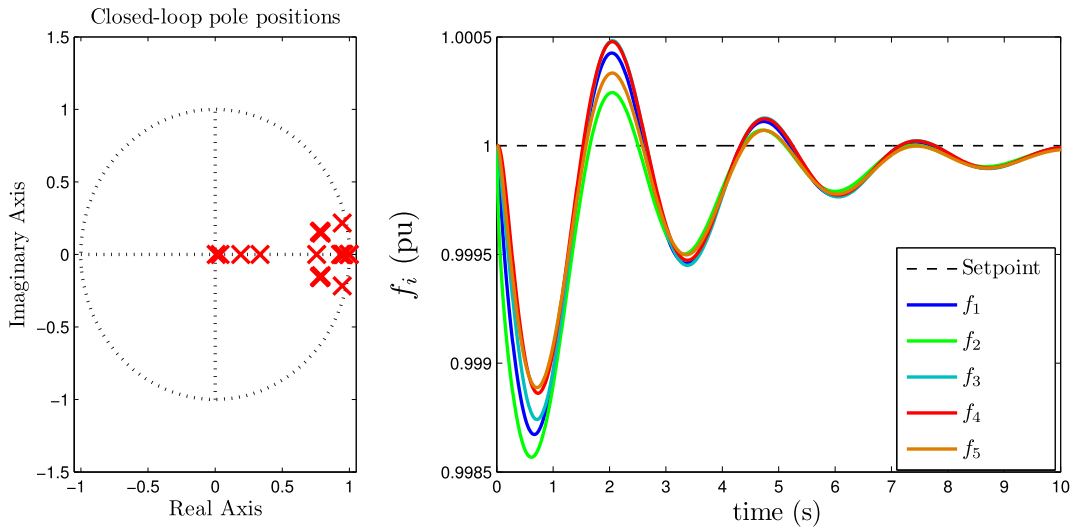

Figure 9: Plot of discrete-time poles and corresponding frequency response for $R_{Pi} = 0.1$.

It is now shown how the eigenvalue analysis can be used to predict the frequencies at which the system will oscillate. Often it can be undesirable for systems to oscillate at certain frequencies, as vibrations at certain frequencies can have undesirable effects on system components, such as creating excessive wear and tear. For $R_{Pi} = 0.1$ the discrete-time eigenvalues are found. These are then converted to the continuous domain where the dominant mode is found at $-0.3006 \pm 2.2495i$. From the analysis, based on a linearisation of the nonlinear system, this predicts that the system should oscillate with a period of about 2.79 s. When the period of oscillation is measured from the nonlinear system simulation, it is shown to oscillate with a period of roughly 2.7 s, which is in good agreement with the predicted value. The contribution of the other non-dominant poles and the effects of system nonlinearities could account for the small discrepancy between the predicted and measured period of oscillation.

8 Conclusions and future work

In this paper the use of a distributed Model Predictive Control (MPC) technique, based on the Auxiliary Problem Principle (APP), is proposed for the implementation of Automatic Generation Control (AGC) in AC areas connected to a Multi Terminal high voltage Direct Current (MTDC) grid. Additionally a modal analysis technique is proposed for the distributed MPC, which was also used for a convergence and stability analysis of the closed-loop system. Results illustrate that stabilising integral control is provided by the distributed MPC, and that the modal analysis technique accurately predicts the modal behaviour of the system.

In future work the technique proposed in this paper could be used in tuning algorithms, such as the distributed MPC tuning algorithm given in Mc Namara, Negenborn, De Schutter, and Lightbody (2013), to achieve desirable closed-loop behaviour. It is also of interest to investigate the utility of distributed MPC for MTDC grids in which there are several points of connection in parallel to individual AC grids, as this more general configuration is anticipated in many MTDC grid deployments.

Acknowledgement

This work was funded by Science Foundation Ireland (Grant 09/ SRC/E1780) as part of the Sustainable Electrical Energy Systems (SEES) research cluster, the Irish Research Council for Science, Engineering and Technology (IRCSET), and supported by the VENI project "Intelligent multi-agent control for flexible coordination of transport hubs" (project 11210) of the Dutch Technology Foundation STW.

References

Andreasson, M., Nazari, M., Dimarogonas, D. V., Sandberg, H., Johansson, K .H., & Ghandhari, M. (2013). Distributed voltage and current control of multi-terminal high-voltage direct current transmission systems. In *Proceedings of the 19th IFAC World Congress*, Cape Town, South Africa, August.

Arnold, M., Negenborn, R. R., Andersson, G., & De Schutter, B. (2009). Multi-area predictive control for combined electricity and natural gas systems. In *Proceedings of the European Control Conference*, Budapest, Hungary, August.

Beerten, J., Cole, S., & Belmans, R. (2014). Modeling of multi-terminal VSC HVDC systems with distributed DC voltage control. *IEEE Transactions on Power Systems*, 29(1), 34-42.

Bertsekas, D. P., & Tsitsikilis, J. N. (1989). *Parallel and distributed computation: Numerical methods* (1st edition). New Jersey, USA: Prentice Hall.

Boyd, S., & Vandenberghe, L. (2009). *Convex optimization.* Cambridge, UK: Cambridge University Press.

Camponogara, E., Jia, D., Krogh, B. H., & Talukdar, S. (2002). Distributed model predictive control. *IEEE Control Systems Magazine*, 22(February (1)), 44-52.

Castillo, E., Minguez, R., Conejo, A. J., & Garcia-Bertrand, R. (2006). *Decomposition techniques in mathematical programming.* New York, USA: Springer.

Censor, Y. (1997). *Parallel optimization: Theory, algorithms, and applications.* New York, USA: Oxford University Press.

Chaudhuri, N., Chaudhuri, B., Majumder, R., & Yazdani, A. (2014). *Multi-terminal direct-current grids: Modeling, analysis, and control.* New York, USA: John Wiley & Sons.

Chaudhuri, N. R., Majumder, R., & Chaudhuri, B. (2013). System frequency support through multi-terminal DC (MTDC) grids. *IEEE Transactions on Power System*, 28 (1), 347-356.

Cole, S., Beerten, J., & Belmans, R. (2010). Generalized dynamic VSC MTDC model for power system stability studies. *IEEE Transactions on Power Systems*, 25(3), 1655-1662.

Dai, J. (2011). *Frequency control coordination among non-synchronous AC areas connected by a multi-terminal HVDC grid* (PhD thesis). France: Supélec.

Dai, J., Phulpin, Y., Sarlette, A., & Ernst, D. (2010). Impact of delays on a consensusbased primary frequency control scheme for AC systems connected by a multiterminal HVDC grid. In *Proceedings of the iREP Symposium on Bulk Power System Dynamics and Control* (pp. 1-9).

Dai, J., Phulpin, Y., Sarlette, A., & Ernst, D. (2012). Coordinated primary frequency control among non-synchronous systems connected by a multi-terminal highvoltage direct current grid. *IET Generation, Transmission, Distribution*, 6(2), 99-108.

de Courreges d'Ustou, B. (2012). *Optimal control design for multiterminal HVDC* (PhD thesis). University of Pittsburgh.

Egea-Alvarez, A., Bianchi, F., Junyent-Ferre, A., Gross, G., & Gomis-Bellmunt, O. (2013). Voltage control of multiterminal VSC-HVDC transmission systems for offshore wind power plants: Design and implementation in a scaled platform. *IEEE Transactions on Industrial Electronics*, 60(6), 2381-2391.

Egea-Alvarez, A., Beerten, J., Van Hertem, D., & Gomis-Bellmunt, O. (2015). Hierarchical power control of multiterminal HVDC grids. *Electric Power Systems Research*, 121, 207-215.

ENTSO-E (2004). *Continental Europe operation handbook-appendix 1: Load frequency control and performance.*

Ersdal, A. M., Imsland, L., & Uhlen, K. (2015). Model predictive load-frequency control. *IEEE Transactions on Power Systems*, http://dx.doi.org/10.1109/TPWRS. 2015.2412614.

Farokhi, F., Shames, I., & Johansson, K. H. (2014). Distributed MPC via dual decomposition and alternative direction method of multipliers. In *Distributed model predictive control made easy* (pp. 115-131).

Giselsson, P., Doan, M. D., Keviczky, T., De Schutter, B., & Rantzer, A. (2013). Accelerated gradient methods and dual decomposition in distributed model predictive control. *Automatica*, 49(3), 829-833.

Hermans, R. M., Lazar, M., & Jokic, A. (2010). Almost decentralized Lyapunov-based nonlinear model predictive control. In *American Control Conference* (pp. 39323938), July.

Hermans, R. M., Jokić, A., Lazar, M., Alessio, A., Van den Bosch, P. P. J., Hiskens, I. A., et al. (2012). Assessment of non-centralised model predictive control techniques for electrical power networks. *International Journal of Control*, 85(8), 1162-1177.

Kennel, F., Gorges, D., & Liu, S. (2013). Energy management for smart grids with electric vehicles based on hierarchical MPC. *IEEE Transactions on Industrial Informatics*, 9(3), 1528-1537.

Kundur, P. (1994). *Power system stability and control.* New York: Mc-Graw Hill.

Li, S., Zhang, Y., & Zhu, Q. (2005). Nash-optimization enhanced distributed model predictive control applied to the shell benchmark problem. *Information Sciences*, 170, 329-349.

Liu, J., Chen, X., Muñoz de la Peña, D., & Christofides, P. D. (2010). Sequential and iterative architectures for distributed model predictive control of nonlinear process systems. *AIChE Journal*, 56(8), 2137-2149.

Ma, M., Chen, H., Liu, X., & Allgöwer, F. (2014). Distributed model predictive load frequency control of multi-area interconnected power system. *International Journal of Electrical Power & Energy Systems*, 62, 289-298.

Maciejowski, J. M. (2002). *Predictive control with constraints.* Harlow, England: Prentice Hall.

Maestre, J. M., & Negenborn, R. R. (2014). *Distributed model predictive control made easy.* Dordrecht, Netherlands: Springer.

Mc Namara, P., Negenborn, R. R., De Schutter, B., & Lightbody, G. (2013). Weight optimisation for iterative distributed model predictive control applied to power networks. *Engineering Applications of Artificial Intelligence*, 26(1), 532-543.

Mc Namara, P., Meere, R., O'Donnell, T., & McLoone, S. (2015). Control strategies for Automatic Generation Control over multi-terminal HVDC grids. *International Journal of Electrical Power and Energy Systems*, preprint available at: http://ercdocuments.ucd.ie/dms/public/MTDCLFCMPCELS.pdf, submitted for publication.

Moradzadeh, M., Boel, R., & Vandevelde, L. (2013). Voltage coordination in multiarea power systems via distributed model predictive control. *IEEE Transactions on Power Systems*, 28(1), 513-521.

Moroş Andan, P.-D., Bourdais, R., Dumur, D., & Buisson, J. (2010). Distributed model predictive control based on Benders' decomposition applied to multisource multizone building temperature regulation. In *49th IEEE conference on Decision and Control* (pp. 3914-3919), December.

Negenborn, R. R., De Schutter, B., & Hellendoorn, J. (2008). Multi-agent model predictive control for transportation networks: Serial versus parallel schemes. *Engineering Applications of Artificial Intelligence*, 21(April (3)), 353-366.

Royo, C. B. (2001). *Generalized unit commitment by the radar multiplier method* (PhD thesis). Barcelona, Spain: Departament d'Estadística i Investigació Operativa, Universitat Politecnica de Catalunya.

Sanchez, G., Giovanini, L., Murillo, M., & Limache, A. (2011). Advanced model predictive control. *Distributed model predictive control based on dynamic games* (pp. 1-26), July. InTech, Rijeka, Croatia.

Sarlette, A., Dai, J., Phulpin, Y., & Ernst, D. (2012). Cooperative frequency control with a multi-terminal high-voltage DC network. *Automatica*, 48(12), 3128-3134.

Silva, B., Moreira, C. L., Seca, L., Phulpin, Y., & Peas Lopes, J. A. (2012). Provision of inertial and primary frequency control services using offshore multiterminal HVDC networks. *IEEE Transactions on Sustainable Energy*, 3(4), 800-808.

Vaccarini, M., Longhi, S., & Katebi, M. R. (2009). Unconstrained networked decentralized model predictive control. *Journal of Process Control*, 19(2), 328-339.

Van Hertem, D., & Ghandhari, M. (2010). Multi-terminal VSC HVDC for the European supergrid: Obstacles. *Renewable and Sustainable Energy Reviews*, 14(9), 3156-3163.

Venkat, A. (2006). *Distributed model predictive control: Theory and applications* (PhD thesis). Wisconsin: University of Wisconsin-Madison.

Zhang, L., Harnefors, L., & Nee, H.-P. (2011). Interconnection of two very weak AC Systems by VSC-HVDC links using power-synchronization control. *IEEE Transactions on Power Systems*, 26(1), 344-355.

Zhang, Y., & Li, S. (2007). Networked model predictive control based on neighbourhood optimization for serially connected large-scale processes. *Journal of Process Control*, 17(1), 37-50.

Zheng, Y., Li, S., & Qiu, H. (2013). Networked coordination-based distributed model predictive control for large-scale system. *IEEE Transactions on Control Systems Technology*, 21(3), 991-998.